Atmosphere-Ocean

ISSN: 0705-5900 (Print) 1480-9214 (Online) Journal homepage: https://www.tandfonline.com/loi/tato20

Sensitivity of Ice Drift to Form Drag and Ice Strength Parameterization in a Coupled Ice–Ocean Model

Kamel Chikhar, Jean-François Lemieux, Frédéric Dupont, François Roy, Gregory C. Smith, Michael Brady, Stephen E. L. Howell & Rodrigue Beaini

To cite this article: Kamel Chikhar, Jean-François Lemieux, Frédéric Dupont, François Roy, Gregory C. Smith, Michael Brady, Stephen E. L. Howell & Rodrigue Beaini (2019) Sensitivity of Ice Drift to Form Drag and Ice Strength Parameterization in a Coupled Ice–Ocean Model, Atmosphere-Ocean, 57:5, 329-349, DOI: 10.1080/07055900.2019.1694859

To link to this article: https://doi.org/10.1080/07055900.2019.1694859

Published online: 19 Dec 2019.

Sensitivity of Ice Drift to Form Drag and Ice Strength Parameterization in a Coupled Ice–Ocean Model

Kamel Chikhar[1,*], Jean-François Lemieux[2], Frédéric Dupont[1], François Roy[2], Gregory C. Smith[2], Michael Brady[3], Stephen E. L. Howell[3], and Rodrigue Beaini[4]

[1]*Service Météorologique du Canada, Environnement et Changement Climatique Canada, Dorval, Quebec, Canada*
[2]*Recherche en Prévision Numérique Environnementale, Environnement et Changement Climatique Canada, Dorval, Quebec, Canada*
[3]*Climate Research Division, Environment and Climate Change Canada, Toronto, Ontario, Canada*
[4]*Polytechnique Montréal, Montréal, Quebec, Canada*

[Original manuscript received 25 March 2019; accepted 14 October 2019]

ABSTRACT *A pan-Arctic sea-ice–ocean prediction system is assessed in terms of its ability to predict sea-ice velocity. This system is based on the Regional Ice Ocean Prediction System running operationally at the Canadian Centre for Meteorological and Environmental Prediction. A form drag parameterization is implemented in the system to allow spatially and temporally varying neutral drag coefficients depending on the sea-ice morphological characteristics. Simulated ice velocity is assessed using data from the International Arctic Buoy Programme, as well as ice motion derived from Environment and Climate Change Canada's synthetic aperture radar automated ice-tracking system. Results indicate that introducing the form drag parameterization systematically increases the sea-ice velocity and exacerbates a positive bias in summer already present in the previous version in which constant neutral drag coefficients were used. The ice strength parameterization used in the model rheology is found to affect the simulated ice drift significantly. Introducing modifications to the ice strength formulation and the empirical parameters helped alleviate the ice velocity bias.*

RÉSUMÉ *[Traduit par la rédaction] Nous évaluons un système de prévision « glace marine-océan » couvrant l'Arctique, et ce, en fonction de sa capacité à prévoir la vitesse de la glace de mer. Ce système se fonde sur le Système régional de prévision océan-glace (SRPOG) du Centre de prévision météorologique et environnementale du Canada (CPMEC). Le système comprend une paramétrisation de la traînée de forme, afin de permettre aux coefficients de traînée neutre de varier dans l'espace et dans le temps selon les caractéristiques morphologiques de la glace de mer. Nous évaluons la vitesse simulée des glaces à l'aide des données issues du Programme international des bouées de l'Arctique ainsi que du mouvement des glaces dérivé du système automatisé de suivi des glaces par radar à synthèse d'ouverture d'Environnement et Changements climatiques Canada. Les résultats indiquent que la paramétrisation de la traînée de forme augmente systématiquement la vitesse de la glace de mer et renforce en été un biais positif déjà présent dans la version précédente, qui utilisait des coefficients de traînée neutre constants. La paramétrisation de la résistance de la glace appliquée à la rhéologie du modèle a un impact considérable sur la dérive simulée des glaces. La modification de la formulation de la résistance de la glace et l'ajout de paramètres empiriques ont contribué à l'atténuation du biais de la vitesse de la glace.*

KEYWORDS ice velocity; variable form drag; ice strength; coupled ice–ocean model

1 Introduction

There is currently an increased demand for skilful environmental forecasts over various time scales for the Arctic region and polar regions in general. Among some of their uses, these forecasts can support maritime transport, assist search and rescue operations, and inform local communities about environmental conditions. In an effort to provide reliable environmental forecasts for northern regions, Environment and Climate Change Canada (ECCC) has, over the past few years, developed several environmental prediction systems. The main ice–ocean prediction system used at ECCC is the 1/4° resolution Global Ice Ocean Prediction

*Corresponding author's email: kamel.chikhar@canada.ca

System (GIOPS; Smith et al., 2016, 2018) running at the Canadian Centre for Meteorological and Environmental Prediction (CCMEP) since 2011; GIOPS provides global ice–ocean analyses and is used to produce daily coupled 10-day forecasts. Higher resolution regional prediction systems have also been developed in order to provide refined forecasts over more limited regions. The 1/12° Regional Ice Ocean Prediction System (RIOPS; Dupont et al., 2015) is a pan-Arctic system that provides four 48-hour ice–ocean forecasts per day. Other systems developed at CCMEP are the ice–ocean analysis and forecasting system for the Gulf of St. Lawrence (Smith, Roy, & Brasnett, 2013) and the Water Cycle Prediction System over the Great Lakes and St. Lawrence River watershed (Dupont, Chittibabu, Fortin, Rao, & Lu, 2012; Durnford et al., 2018). All these systems are based on the Nucleus for European Modelling of the Ocean (NEMO) ocean model (Madec, 2008; Madec, Delecluse, Imbard, & Lévy, 1998) and the Los Alamos sea-ice model (CICE; Hunke, Lipscomb, Turner, Jeffery, & Elliott, 2015). They are forced with or coupled to the Global Multiscale Model (GEM) atmospheric model developed at the CCMEP (Côté et al., 1998a; Côté et al., 1998b).

Ice–ocean forecasting systems such as the ones listed above can predict the evolution of many physical fields. In terms of sea ice, some useful forecast fields are concentration, thickness, internal pressure, and ice-velocity. In this paper, we explore some avenues for improving ice-velocity forecasts.

In the current continuum-based sea-ice models, the velocity is simulated according to the two-dimensional sea-ice momentum equation (Hibler, 1979),

$$m\frac{D\mathbf{u}_i}{Dt} = \boldsymbol{\tau}_a + \boldsymbol{\tau}_w + \nabla\cdot\sigma - \mathbf{k}\times mf\,\mathbf{u}_i - mg\nabla H_o, \qquad (1)$$

where m is the total mass of ice and snow per unit area, $\frac{D}{Dt}$ is the total derivative and $\mathbf{u}_i$ is the horizontal sea-ice velocity vector. On the right-hand side, $\boldsymbol{\tau}_a$ and $\boldsymbol{\tau}_w$ are the wind and water stresses respectively, $\nabla\cdot\sigma$ is the internal stress gradient, $\mathbf{k}\times mf\,\mathbf{u}_i$ the Coriolis force, and $mg\nabla H_o$ is the sea surface tilt term. The terms H_o, f, and t are the sea surface height, the Coriolis parameter, and the time, respectively. Finally, $\mathbf{k}$ is a normal unit vector.

In Eq. (1), the main factors constraining sea-ice drift are the wind stress, the water stress, and the internal stress gradient (Bouchat & Tremblay, 2014; Steele, Zhang, Rothrock, & Stern, 1997). Because of the importance of these terms to the simulated ice velocity, they have received much attention from various groups of researchers.

The stresses $\boldsymbol{\tau}_a$ and $\boldsymbol{\tau}_w$ are based on quadratic formulations. They are given, respectively, by,

$$\boldsymbol{\tau}_a = \rho_a\, A_i\, C_{\mathrm{Dai}}\, |\mathbf{u}_a|\, (\mathbf{u}_a\, \cos\phi + \mathbf{k}\times\mathbf{u_a}\, \sin\phi), \qquad (2)$$

and

$$\boldsymbol{\tau}_w = \rho_w\, A_i\, C_{\mathrm{Dwi}}\, |\mathbf{u}_w - \mathbf{u}_i|\, [(\mathbf{u}_w - \mathbf{u}_i)\, \cos\theta + \mathbf{k}\times(\mathbf{u}_w - \mathbf{u}_i)\, \sin\theta)], \qquad (3)$$

where $\mathbf{u}_a$, $\mathbf{u}_w$ and $\mathbf{u}_i$ are the wind, water current, and ice velocity vectors, respectively; ρ_a and ρ_w are the air and water densities; $\mathbf{A}_i$ is the ice concentration, while C_{Dai} and C_{Dwi} are the air and water drag coefficients (transfer coefficients for momentum); and ϕ and θ are the turning angles. Because the wind and water stresses are proportional to the drag coefficients, the accuracy of the simulated ice velocity relies greatly on the way these coefficients are parameterized.

In many ice–ocean models, the neutral drag coefficients (i.e., with neutral surface layer stability) are derived from the logarithmic wind (current) profile assumption and constant roughness length. In our sea-ice–ocean model, the air–ice drag coefficient C_{Dai} used in air stress computation (Eq. (2)) varies depending on the stability of the atmospheric surface layer. In the case of the ice–water drag coefficient C_{Dwi}, the water surface layer stability is not taken into account. However, both coefficients (C_{Dai} and C_{Dwi}) still lack the spatially and temporally changing form drag contribution due to sea-ice morphology (e.g., ridge height, keel depth, and floe size). Moreover, the values of drag coefficients often used in ice–ocean models are derived for low vertical resolution applications (Roy et al., 2015). For a more accurate representation of the air and water stresses, the calculation of the drag coefficients should consider the stability of the atmosphere, the sea-ice morphology, and the fact that ocean models are being run at increasingly higher vertical resolution for which ice-ocean drag coefficients based on geostrophic currents are not appropriate. The fact that the Arctic sea-ice cover is currently shrinking and thinning (e.g., Kwok & Untersteiner, 2011; Stroeve et al., 2012) implies significant changes in the spatial and temporal distribution of sea-ice cover topography (Castellani, Lüpkes, Hendricks, & Gerdes, 2014; Petty et al., 2016). As a response, the ice drift, driven mainly by wind and ocean stresses, is also changing substantially (Hakkinen, Proshutinsky, & Ashik, 2008; Kwok, Spreen, & Pang, 2013). Therefore, an adequate representation of ice morphology characteristics (e.g., ridge height and frequency, distance between floes, and area of melt ponds) is crucial in simulating ice velocity.

Recognizing the importance of topography on turbulent exchanges, many researchers have proposed different parameterizations to take form drag into account. Some of these parameterizations define the drag coefficients based on characteristics of the sea-ice cover (e.g., Lüpkes, Gryanik, Hartmann, & Andreas, 2012; Tsamados et al., 2014), and others relate the surface roughness to the deformation energy and ice concentration (e.g., Castellani, Losch, Ungermann, & Gerdes, 2018; Steiner, 2001).

Tsamados et al. (2014) introduced a new drag parameterization that explicitly takes the ice morphology into account to compute neutral drag coefficients for ice–atmosphere and ice–ocean interfaces. This form drag parameterization, used in this study, has been included in version 5 of the CICE sea-ice model (Hunke et al., 2015). In this parameterization, the total neutral air–ice and ice–ocean drag coefficients are estimated through separate contributions from different ice

characteristics. That is,

$$C_{\mathrm{dna}} = C_{\mathrm{dna\_ridge}} + C_{\mathrm{dna\_floe}} + C_{\mathrm{dna\_pond}} + C_{\mathrm{dna\_skin}}, \quad (4)$$

where C_{dna} is the total neutral air–ice drag coefficient and, $C_{\mathrm{dna\_ridge}}$, $C_{\mathrm{dna\_floe}}$, $C_{\mathrm{dna\_pond}}$, and $C_{\mathrm{dna\_skin}}$ are the contributions from ridges, floes, melt ponds, and level ice, respectively.

In a similar way, the total neutral ice-ocean drag coefficient (C_{dnw}) is given by,

$$C_{\mathrm{dnw}} = C_{\mathrm{dnw\_ridge}} + C_{\mathrm{dnw\_floe}} + C_{\mathrm{dnw\_skin}}, \quad (5)$$

where C_{dnw} is the sum of the keel ($C_{\mathrm{dnw\_ridge}}$), floe ($C_{\mathrm{dnw\_floe}}$), and level ice ($C_{\mathrm{dnw\_skin}}$), contributions. A detailed description of these coefficients can be found in Tsamados et al. (2014). In summary, these coefficients are estimated from different ice topographic characteristics, such as ridge height, keel depth, floe size, melt pond size, distance between ridges or floes. All the parameters describing ice surface morphology features are derived from model prognostic variables, such as ice concentration, ice thickness, and ridged ice volume. Consequently, this parameterization allows the neutral drag coefficients to evolve in time and space.

The internal ice stress gradient in Eq. (1), often referred to as the rheology term, is another important factor affecting simulated ice velocity. Although new sea-ice rheologies have been developed recently (e.g., Girard et al., 2011; Schreyer, Sulsky, Munday, Coon, & Kwok, 2006; Tsamados, Feltham, & Wilchinsky, 2013), most sea-ice models are still based on the viscous-plastic rheology. Finding the most appropriate rheological framework for modelling sea ice is still the subject of intense research and debate (e.g., Bouchat & Tremblay, 2017; Girard et al., 2011; Hutter, Losch, & Menemenlis, 2018). An essential characteristic of sea-ice rheology is ice strength. In current sea-ice models, two main approaches are used to parameterize ice strength, one is based on Hibler (1979) and the other on Rothrock (1975). In Hibler (1979), ice strength is formulated as a linear function of mean ice thickness and an exponential function of ice concentration. Rothrock (1975) proposes a more complex formulation by considering the potential energy gain and the frictional energy loss through the ridging process. In both strength parameterizations, many assumptions are made, for example in the empirical parameters, because of missing observations or lack of scientific knowledge. Consequently, uncertainties remain significant, and active research is ongoing in this field to improve ice strength modelling (Ungermann, Tremblay, Martin, & Losch, 2017).

The first objective of this study is to investigate the performance of the CICE–NEMO coupled ice–ocean prediction system, focusing specifically on the simulated ice drift when the form drag parameterization is implemented, that is, when ice topography is explicitly parameterized. Tsamados et al. (2014) and Martin, Tsamados, Schroeder, and Feltham (2016) studied the effect of variable neutral drag coefficients at the air–ice and ice–ocean interfaces on simulated sea-ice characteristics. They found significant differences from the case in which neutral drag coefficients are kept constant over the model domain and during the length of the simulation. In these studies, they used a sea-ice model run in stand-alone mode (i.e., forced both at the air–ice and the ice–ocean interfaces). Here, the impact of the variable form drag parameterization of Tsamados et al. (2014) is instead examined in the context of a sea-ice model coupled to an ocean model. This is a major difference in that the variable ice–ocean form drag introduces additional effects through coupled interactions (feedbacks) with the ocean model. Note that Castellani et al. (2018) studied the impact of a form drag parameterization based on deformation energy (Steiner, 2001) in the MITgcm coupled ice–ocean modelling framework. Compared with their reference simulation with constant drag coefficients, their simulation with form drag exhibits a thinner and faster sea-ice cover. They also obtained a deeper ocean mixed layer, especially during summer.

The second objective of this study is to explore how different ice strength formulations affect model ice dynamics and how this is reflected in simulated ice drift.

This paper is organized as follows. Descriptions of the ice–ocean model used and the adopted methodology are given in Section 2. Results are presented and discussed in Section 3. Finally, conclusions are provided in Section 4.

2 Experimental setup

a *Sea-Ice–Ocean Model Description*

In this study, we use CICE (version 5) with 10 ice-thickness categories coupled to the NEMO ocean model (version 3.6) in a 1/4° resolution pan-Arctic configuration derived from a global tripolar grid such that grid spacing in the Arctic is between 10 and 15 km. The coupled ice–ocean model configuration used in this study is based on RIOPS but with a coarser horizontal resolution and without tides. Other parameters and model settings are as in Dupont et al. (2015).

The atmospheric forcing applied comes from the Canadian Global Deterministic Prediction System (Charron et al., 2012) Reforecasts (CGRFs) (Smith et al., 2014) based on the GEM atmospheric model. The ice–ocean model is forced by wind, temperature, specific humidity, precipitation, and radiation fluxes taken from the lowest atmospheric model level (∼40 m). More information on the atmospheric forcing method can be found in Roy et al. (2015). It should be noted that in our sea-ice model, ice velocity is simulated using a modified version of Eq. (1) to which an additional term $\boldsymbol{\tau}_b$ is introduced representing the seabed stress term due to grounded ridges following Lemieux et al. (2016). Note that this term can only be non-zero in shallow water (less than 30 m).

In order to assess the impact of the new form drag coefficients, two test simulations are carried out. In the first simulation, we use constant neutral drag coefficients based on roughness lengths. In addition, following Roy et al. (2015),

the reference depth for the ocean current used in the calculation of the water stress is set to 0.5 m (this corresponds to the mid-point of the first vertical layer in the NEMO model). Although the neutral drag coefficients are constant in space and time, the atmospheric drag coefficient can vary depending on the stability of the atmospheric surface layer. This formulation of drag coefficients is currently used in all our operational systems (RIOPS, GIOPS, etc.). In the second simulation, the neutral drag coefficients follow the formulation of Tsamados et al. (2014) and, therefore, take into account ice morphology. All parameters used in the form drag parameterization are identical to those used in Table 2 of Tsamados et al. (2014). However, as opposed to the reference ocean depth of 10 m used by Tsamados et al. (2014), it is set to 0.5 m here (consistent with the first run). The ice–atmosphere and ice–ocean level ice roughness lengths are also different and set to 5.7×10^{-5} m, and 6.0×10^{-3} m, respectively. The ice–atmosphere roughness length value results from a minimization procedure detailed in Section 2.c, while the ice–ocean roughness is taken from McPhee (2002). Moreover, as in the first simulation, the atmospheric drag coefficient depends on the stability of the atmospheric surface layer. Because near-surface ocean currents and winds are used in the formulation of the stresses, the turning angles in Eqs (2) and (3) are set to zero for all our simulations.

In our CICE version, a viscous-plastic (VP) rheology is used with an elliptical yield curve (Hibler, 1979). Following the study of Lemieux et al. (2016), the ellipse aspect ratio is set to 1.5, and a small amount of isotropic tensile strength is added ($k_t = 0.05$). These values were found to improve landfast ice simulation. In addition, the Hibler ice strength formulation (Hibler, 1979) is used rather than that of Rothrock (Rothrock, 1975), the CICE default formulation. Indeed, we found that RIOPS simulations using the Rothrock ice strength formulation tend to produce unrealistically large thicknesses in tidally active regions (higher than 10 m in some places). Reverting to Hibler's formulation mitigated these extreme values. Hence, Hibler formulation was chosen in the operational implementation. Ungermann et al. (2017) also compared the two ice strength parameterizations and found that more accurate simulations are obtained with Hibler's formulation. More details about changes to the ice rheology and the landfast ice parameterization used in our CICE configuration can be found in Lemieux et al. (2016).

b *Ice Velocity Validation Method*

The simulated sea-ice velocity is validated through a comparison with data coming from two datasets. The first dataset used comes from the International Arctic Buoy Programme (IABP) (Rigor & Ortmeyer, 2004). This network provides drifting buoy positions over a 12-hour time interval. This dataset is frequently used by the sea-ice modelling community to assess simulated sea-ice velocity (e.g., Hakkinen et al., 2008; Hebert et al., 2015; Kreyscher, Harder, Lemke, & Flato, 2000).

The IABP data are first quality controlled and filtered following several conditions. First, we consider buoy positions at a 24-hour time interval (e.g., day D at 0000 UTC to day D + 1 at 0000 UTC). Furthermore, buoy data are used only when the initial position corresponds to a model grid point where the simulated ice concentration is at least 50%. Additional filtering is applied by ignoring buoys with 24-hour mean velocity reaching or exceeding 1 m s^{-1}. This rejection criterion results from ocurrence frequency investigation on all buoys located on grid points where sea-ice concentration is at least 50%. This additional filter eliminates a very small number of buoys (0.03%) and is useful for rejecting (some) defective buoys. Such filters are applied to ensure that the buoys considered are not floating on water or defective. The "observed" 24-hour mean velocity is retrieved by computing the distance covered between the final and initial positions on the sphere using the Haversine formula with a constant earth radius (6371 km) and dividing by the time interval. The second dataset used to validate ice drift is the Automated Sea Ice Tracking System (ASITS) data derived from sequential synthetic aperture radar RADARSAT-2 ScanSAR images (Komarov & Barber, 2014). This ice system has been used previously to understand long-term changes in Arctic sea-ice dynamics (e.g., Howell et al., 2013). The root mean square error in the RADARSAT-2 ice motion tracking displacement when compared with buoy data is 0.43 km (Komarov & Barber, 2014). This dataset consists of ice-feature tracking using pairs of images at different time intervals and for different dates. A detailed description of this ice motion tracking algorithm can be found in Komarov and Barber (2014). These data are also quality controlled and only those at the maximum confidence level are taken into account. Also, we only use displacements corresponding to time intervals of more than 6 h and less than 48 h. The procedure for retrieving observed ice velocity is similar to that used for the IABP buoy data with the exception that the time interval is no longer constant (24 h) but varies from 6 to 48 h. Similar to the buoy data, we use initial and final positions and time intervals and retrieve the observed ice velocity by computing the distance covered on a sphere divided by the time interval. It should be noted, however, that the ASITS data used in this study cover only the Beaufort Sea region while the IABP buoy data cover a wider region of the Arctic Ocean.

In order to compute the velocity bias, for each IABP buoy and ASITS dataset, the corresponding "simulated" ice velocity is computed using a Lagrangian particle dispersion model (Modèle Lagrangien de dispersion de particules (MLDP); Flesch, D'Amours, Mooney, & Wilson, 2004) used by the Environmental Emergency Response Section at the CCMEP. More precisely, the MLDP model takes the observed buoy or ice particle initial position and performs a Lagrangian drift using 3-hourly predicted ice velocities from CICE. The final position is then obtained and used to compute the mean simulated ice velocity over the time interval between the original and final positions. Finally, for each consecutive date, the mean bias is computed by averaging individual biases from all

buoys or ASITS data considered, as

$$\text{bias} = < |\mathbf{v}_{mi}| - |\mathbf{v}_{bi}| >, \tag{6}$$

where $\mathbf{v}_{mi}$ and $\mathbf{v}_{bi}$ are, respectively, the simulated and observed velocity vectors as defined previously. Here, we use $\langle\rangle$ symbols as an averaging notation.

A more complete validation diagnostic metric that we call vdiff is defined as

$$\text{vdiff} = < |\mathbf{v}_{mi} - \mathbf{v}_{bi}| >. \tag{7}$$

While the bias gives information about differences in magnitude of the observed and simulated velocity, vdiff characterizes the magnitude of the difference between the observed and simulated drift vectors. Namely, it represents the mean velocity computed using the distance between the observed and simulated final positions. The vdiff metric gives implicit information on the deviation between the simulated and observed ice drift. Assuming a small velocity bias, high vdiff values denote large directional departures between the simulated and observed ice drift directions.

c *Simulations*

In the first part of this study, we investigate the impact of the form drag parameterization on the simulated sea ice. First, a 3-year (2001–2004) model spin-up run is achieved using the form drag parameterization with default configuration. This run is initialized using ice thickness and concentration from the Global Ocean Reanalysis and Simulations (Glorys2v1; Ferry et al., 2012). Initial and lateral conditions come from the Mercator Ocean ORCA12-T321 simulation providing the ocean inflow at Bering Strait. In addition, Bering Strait is considered a closed boundary for sea ice. To obtain a realistic reference simulation, an optimization procedure for the sea-ice velocity bias was conducted over a 3-year period (September 2004 to September 2007). To do so, the ice–atmosphere roughness length (used in the calculation of $C_{\text{dna\_ridge}}$ and $C_{\text{dna\_skin}}$ in Eq. (4)) is adjusted using the IABP data over the 3-year period in order to minimize the mean bias. This approach is motivated by the uncertainty existing in the atmospheric forcing imposed on the system. Based on this minimization procedure, the ice–atmosphere roughness length is set to 5.7×10^{-5} m. It is stressed here that this minimization procedure is just a preliminary step to provide a relatively unbiased reference simulation.

Using the optimized ice–atmosphere roughness length, a reference hindcast simulation that covers an extended period from September 2004 to December 2010 was conducted. This form drag reference simulation referred to as the form drag reference simulation (FDRS) is initiated from a restart that comes from the model spin-up run. For the purposes of comparison, another simulation was performed over the same period (September 2004 to December 2010) with neutral drag coefficients kept constant as is done currently in GIOPS or RIOPS (and most other ice–ocean models). We will refer to this simulation as the constant neutral drag simulation (CNDS). The values of the constant coefficients in CNDS are chosen such that, under the hypothesis of neutral surface stability, the total stress averaged spatially and temporally over the entire domain and simulation period are assumed equivalent in both FDRS and CNDS runs.

The procedure used to determine the constant coefficients values in CNDS is detailed in the following.

Using FDRS outputs, the mean neutral drag coefficient for the ice–atmosphere interface can be obtained from Eq. (8),

$$\langle\overline{C_{\text{dna}}}\rangle = \frac{\sum_{t=0}^{T}\sum_{j=0}^{N} A_j^t\ S_j^t\ C_{\text{dna}_j}^t\ \mathbf{u}_{a_j}^{t\ 2}}{\sum_{t=0}^{T}\sum_{j=0}^{N} A_j^t\ S_j^t\ \mathbf{u}_{a_j}^{t\ 2}}, \tag{8}$$

where A_j^t is the ice concentration, S_j^t is the grid cell area, $C_{\text{dna}_j}^t$ is the simulated (variable) ice–atmosphere neutral drag coefficient, $\mathbf{u}_{a_j}^t$ is the wind, N is the total number of model grid points where the ice concentration is above 15% and, T is the total number of model outputs, typically 3-hourly during the simulation period length.

In the same manner, using FDRS outputs, the mean ice–ocean neutral drag coefficient can be obtained from Eq. (9) where $C_{\text{dnw}_j}^t$ is the simulated ice–ocean drag coefficient, $\mathbf{u}_{w_j}^t$ and $\mathbf{u}_{i_j}^t$ are ocean current and ice velocity, respectively.

$$\langle\overline{C_{\text{dnw}}}\rangle = \frac{\sum_{t=0}^{T}\sum_{j=0}^{N} A_j^t S_j^t C_{\text{dnw}_j}^t |\mathbf{u}_{w_j}^t - \mathbf{u}_{i_j}^t|^2}{\sum_{t=0}^{T}\sum_{j=0}^{N} A_j^t S_j^t |\mathbf{u}_{w_j}^t - \mathbf{u}_{i_j}^t|^2}. \tag{9}$$

Once the mean neutral drag coefficients have been obtained, we can deduce a mean roughness length for ice–atmosphere and ice–ocean interfaces. This is achieved from the neutrally stratified surface layer theory for which the surface drag coefficient is expressed as

$$C_{\text{dn}} = \kappa^2 \left[\log\left(\frac{z_{\text{ref}}}{z_0}\right)\right]^{-2}, \tag{10}$$

where z_{ref} is a reference height or depth (in our case it is set to 10 and 0.5 m for the ice–atmosphere and ice–ocean interfaces, respectively), z_0 is the roughness length, and κ the von Karman constant.

The roughness length is finally deduced as

$$z_0 = z_{ref}\left[exp\left(\frac{\kappa}{C_{\text{dn}}^{\frac{1}{2}}}\right)\right]^{-1}. \tag{11}$$

Using Eqs (8) and (9) gives $\langle\overline{C_{\text{dna}}}\rangle = 0.00167$ and $\langle\overline{C_{\text{dnw}}}\rangle = 0.0146$ and, consequently, from Eq. (11), the ice-atmosphere and ice-ocean roughness lengths applied to the

CNDS will be $z_{0_{ia}} = 5.7 \times 10^{-4}$ m and $z_{0_{iw}} = 1.82 \times 10^{-2}$ m, respectively.

In the second part of the study based on extensive sensitivity tests, we investigate ways to improve simulated ice drift. All these additional simulations use the form drag parameterization. They are initialized from the same restart valid on 23 December 2008 and cover the next year (2009). The simulation length is set to one year in order to limit the computing cost that would otherwise be too expensive.

3 Results

In the next subsections, we present results from the model simulation in which the new form drag parameterization was applied. For descriptive purposes, in the first subsection, we evaluate some general ice features resulting from the FDRS simulation, considered as the "reference run," but also those from CNDS. The modelled ice features are compared with several datasets, such as those from the National Snow and Ice Data Center (NSIDC, version 2; Fowler, Maslanik, Emery, & Tschudi, 2013) and Ice, Cloud, and Land Elevation Satellite (ICESat) retrievals (Kwok et al., 2009). In the second subsection, FDRS results are described through the different contributions to the drag coefficients at both air–ice and water–ice interfaces. The third subsection is devoted to the impact of form drag parameterization on ice velocity, while the fourth one deals with the model sensitivity to changes in the form drag parameterization. Finally, the fifth subsection presents results from tests on ice strength formulation and how it affects the simulated ice velocity.

a *General Simulated Ice Features*

As mentioned previously, hindcast simulations with the form drag option activated (FDRS) or not (CNDS) are performed for approximately a 6-year period (from September 2004 to December 2010). In this subsection, we briefly analyze some general ice characteristics as simulated by our system. First, the total Arctic sea-ice volume temporal evolution from the FDRS and CNDS is presented in Fig. 1. It can be seen that the ice volume decreases with time in both the FDRS and CNDS simulations with a similar trend. However, we observe a lower ice volume with FDRS with the differences becoming more noticeable as the simulation progresses. Furthermore, the total ice cover over the Arctic (not shown) exhibits a lower September minimum in FDRS compared with CNDS. In addition, Lemieux et al. (2018) used a model version similar to CNDS and compared the simulated total sea-ice volume to that from the Pan-Arctic Ice–Ocean Modeling and Assimilation System (PIOMAS; Schweiger et al. (2011)). They found that the model is in quite good agreement with PIOMAS in terms of volume and trend (their model exhibits slightly higher volume, especially in summer).

An important sea-ice variable to look at is ice concentration. The simulated monthly means for March and September are presented in Fig. 2. Results show that the model simulations are in good agreement with NSIDC data. Comparison between FDRS and CNDS September averages reveals some differences, especially to the north of the Canadian Arctic Archipelago (CAA) where more ice cover is observed in CNDS. However, compared with NSIDC data, the two simulations exhibit less ice concentration.

The third analyzed characteristic is sea-ice thickness, which is an essential prognostic variable. The simulated ice thickness averaged over two periods (October–November 2007 and February–March 2008) is presented in Fig. 3 where FDRS and CNDS results are compared with ICESat retrievals. Considering the February–March period, the comparison with ICESat data indicates that the simulated ice thickness is in agreement over the majority of the model domain. However, we observe an overestimation in both FDRS and CNDS to the north of Greenland and the CAA. Similarly, results from the October–November period show thicker ice in both the

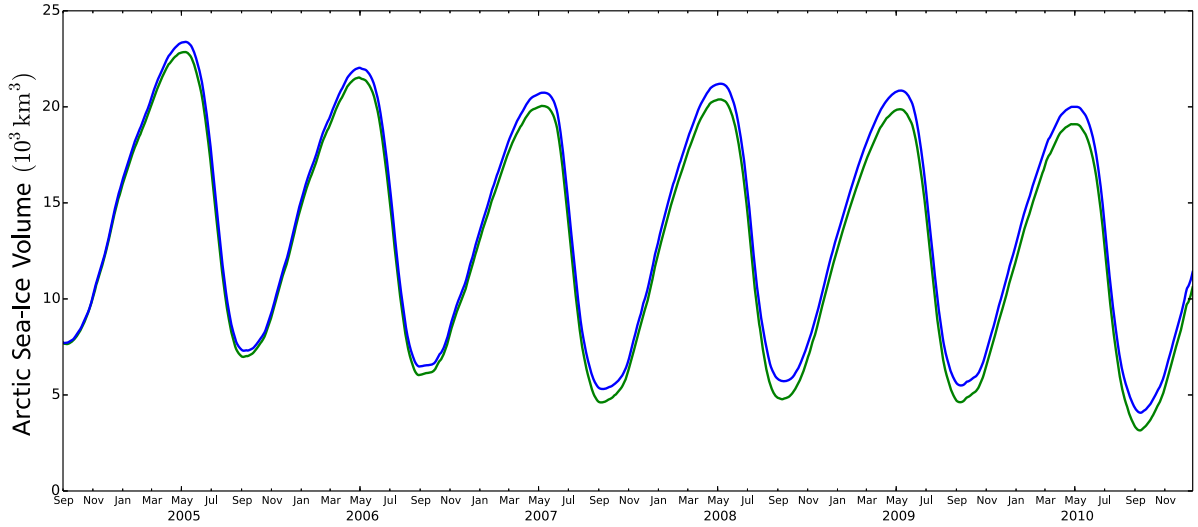

Fig. 1 Arctic total sea-ice volume as simulated by the FDRS (green line) and the CNDS (blue line).

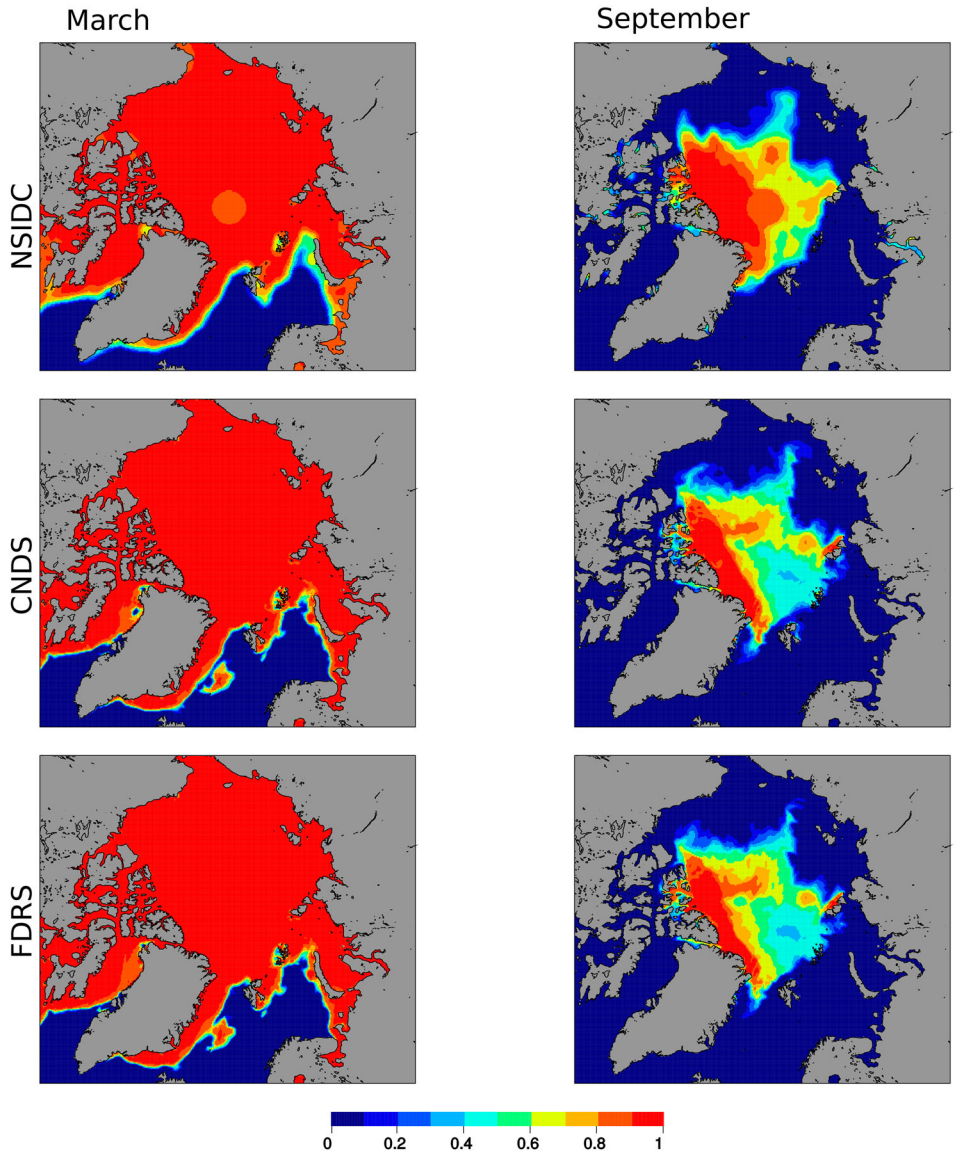

Fig. 2 Monthly mean (2004–2010) sea-ice concentration for March (left panels) and September (right panels). NSIDC data is shown in the top row while the middle and bottom rows show CNDS and FDRS results, respectively.

FDRS and CNDS to the north of Greenland. However, both simulations seem to underestimate ice thickness to the north of the CAA. Comparing FDRS and CNDS reveals clearly thinner ice in FDRS for both periods, especially north of the CAA and Greenland. This is consistent with the sea-ice volume temporal evolution presented in Fig. 1. The thinner ice thickness in FDRS is also in agreement with the findings of Castellani et al. (2018).

Finally, an overall overview of ice drift is presented in Fig. 4 where the two simulations (CNDS and FDRS) are compared with NSIDC estimates. The ice drift is averaged between November and April as in Sumata et al. (2014) who found that the NSIDC product is more accurate during this winter period. The main ice dynamic features, such as the Beaufort Gyre and the Transpolar Drift Stream, are qualitatively in good agreement with the NSIDC product. It is, however, noticed that the ice drift is much faster in both CNDS and FDRS, especially in the Beaufort Gyre, as well as the transpolar drift through Fram Strait. It is stressed here that this comparison is qualitative and version 2 of the NSIDC data used in this model validation exhibits lower ice velocity compared with other validation products and IABP buoys especially in summer (Sumata et al., 2014).

b *The Reference Run*

Following Tsamados et al. (2014), we examine the contribution to the total neutral drag coefficient of the different components related to ice topography features, namely ridges and keels, floe edges, melt ponds edges, and the level ice. The contribution from these different components is presented in Fig. 5 for the ice–atmosphere (top) and ice–ocean (bottom) interfaces.

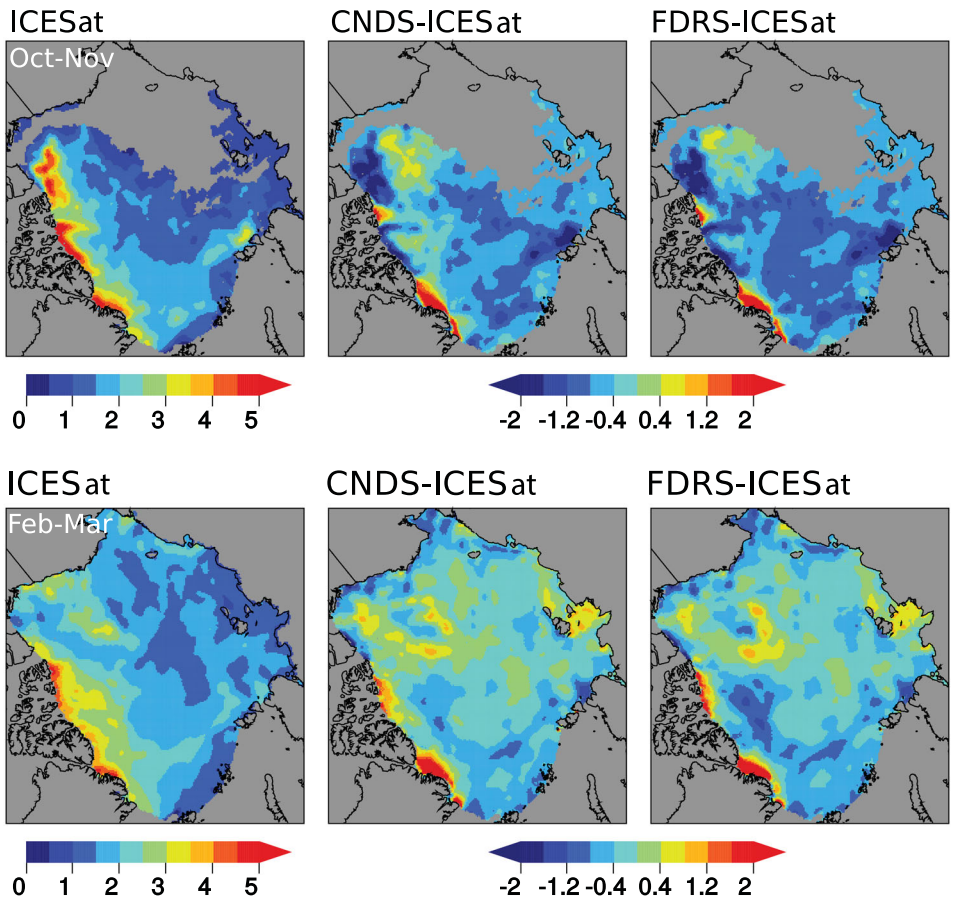

Fig. 3 Sea-ice thickness in metres averaged over October–November 2007 (top) and February–March 2008 (bottom). Differences are indicated in the rightmost panels.

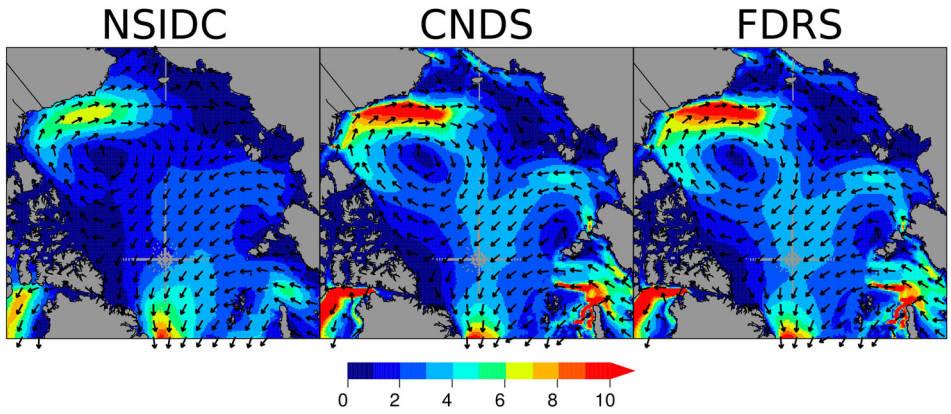

Fig. 4 Average sea-ice drift (2004–2010) in cm s^{-1} from NSIDC estimates (left), CNDS (middle), and FDRS (right). The drift is averaged over the period between November and April. The intensity and direction are shown in colours and vectors, respectively.

In our simulation, the maximum total neutral drag coefficient for the two interfaces occurs in June. Results also show that the two predominant contributions come from ridges and keels and level ice throughout most of the year because their combined contributions exceed 95%. However, in the summer season, contributions from floe edges become more significant especially for the ice–ocean interface where the neutral drag coefficients become comparable to those from the keels (more than 40% in August). The melt ponds only contribute to the total form drag between May and September. On average and over the entire Arctic, it accounts for approximately 10% of the total drag during the June to August period.

A qualitative comparison between our results and those of Tsamados et al. (2014) reveals a temporal phase difference

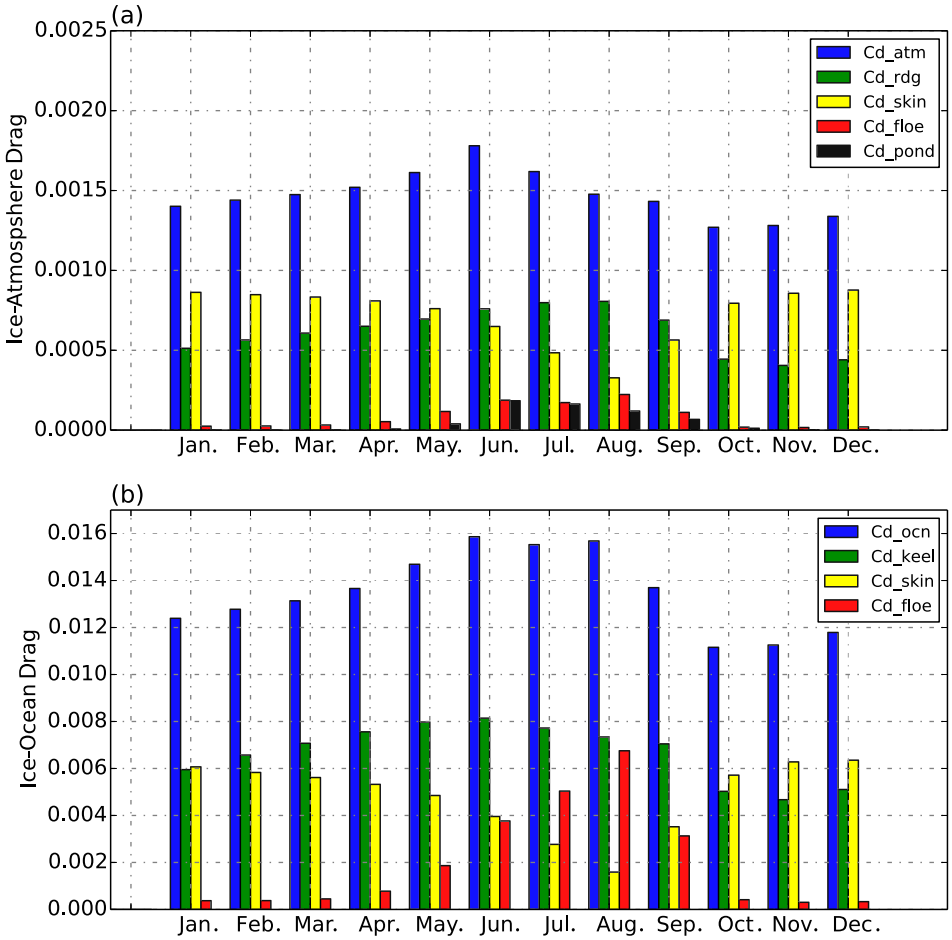

Fig. 5 Contribution to the total neutral form drag (blue) from different components for (a) the ice–atmosphere and (b) the ice–ocean interfaces. The neutral drag coefficients are averaged over the model domain for grid cells where the ice concentration is more than 15%. Drag coefficients presented show contribution from ridges and keels (green), floe edge (red), melt ponds edge (black), and level ice (yellow).

in the neutral drag coefficient maximum for the ice–atmosphere interface from August in their study to June in our case. For the ice–ocean interface, we observe a maximum extending from June to August. In addition, our model exhibits higher neutral drag coefficient values for the ice–ocean interface, which is consistent with the modification of the reference depth from 10 m to 0.5 m as mentioned in Section 2.a.

Another interesting aspect of the form drag to examine is spatial variability. As an example, Fig. 6 shows the June monthly mean total drag coefficients, as well as contributions from the different components. Figure 6 shows that the maximum drag for the two interfaces occurs in the region north of Greenland and the CAA with values exceeding 3.0×10^{-3} and 2.5×10^{-2} for the ice–atmosphere and ice–ocean interfaces, respectively. Figure 6 also shows the predominance of the ridge and keel drags shown in Fig. 5 and illustrates that the drag from these ice features exists not only to the north of Greenland and the CAA but also off the coast of Alaska. The drag from floe edges (freeboard and draft) is also significant, especially at the ice–ocean interface and exists mainly west of the CAA and along the Alaskan coast where the ice fails under tension and shear causing more frequent leads and cracks. The floe-edge drag is also well noted in the Fram Strait region where leads appear rapidly in the accelerating ouflowing ice drift. The drag from melt pond edges is found to be predominant to the north of Greenland and the CAA where high and large ridges promote melt pond formation. Finally, the level ice drag is mostly significant in the central Arctic ice pack.

As mentioned previously, one objective of this study is to investigate the impact of the form drag parameterization on the simulated ice drift. A preliminary exploration is presented in the next subsection where the addition of form drag (FDRS) is compared with the previous model version in which neutral drag coefficients are considered to be constant (CNDS).

c *The Impact of Form Drag on Ice Velocity*

In the following, we compare results obtained from FDRS and CNDS as defined in Section 2.c with IABP and ASITS data. The constant neutral drag coefficients used in CNDS are obtained as explained in Section 2.c. The ice velocity bias (bias) and the directional deviation induced from vdiff, as described in Section 2.b, are computed, in the case of IABP data over the entire Arctic (north of 70°N) and over two

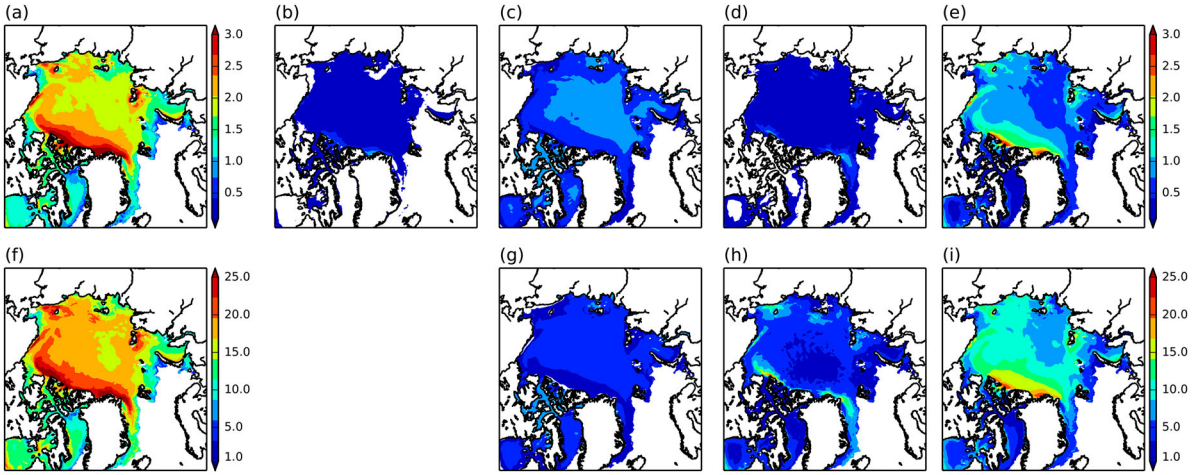

Fig. 6 June monthly-mean spatial distribution of the total neutral drag coefficient. The top panels denote (a) the ice–atmosphere total neutral drag coefficient and its contributions from (b) melt pond edges, (c) level ice, (d) floe edge freeboard, and (e) ridges. The bottom panels represent (f) the ice–ocean total neutral drag coefficient, (g) contribution from level ice drag, (h) floe edge draft, and (i) keels. Values are multiplied by 1000.

separate regions, namely the Beaufort Sea region and north of the CAA and Greenland as shown in Fig. 7. The choice of these regions is justified not only by their very different ice dynamics but also by the availability of buoy data. North of the CAA and Greenland, the ice is more rigid and relatively thick throughout the year, whereas in the Beaufort Sea region the ice is thinner and more mobile, especially during the summer period (Richter-Menge & Farrell, 2013). As shown in Fig. 7, the southern limit for the two regions is moved away from the shore to consider only drifting buoys and avoid those that may be located on landfast ice and thus immobile.

The resulting diagnostics are presented in Fig. 8 and summarized in Tables 1 and 2 for which summer and winter

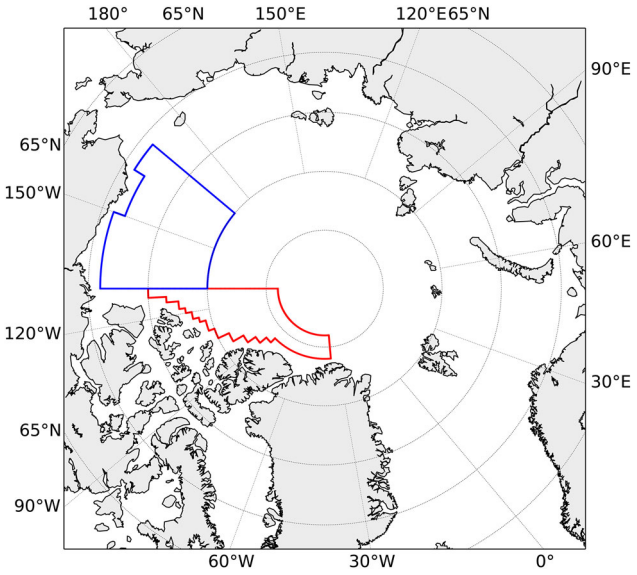

Fig. 7 Subregions used in ice velocity diagnostics computation. The region north of the Canadian Arctic Archipelago and Greenland is outlined by the red line and the Beaufort Sea region by the blue one.

represent the periods from June to August and September to May, respectively. We observe from Fig. 8 and Tables 1 and 2 that the ice-drift velocity is systematically increased in FDRS. As a result, a positive summertime bias, already existing in the CNDS, is exacerbated. Moreover, we observe a rapid transition in the bias in both cases (FDRS and CNDS), shifting rapidly from positive values during the summer period to negative ones in the fall. A deeper analysis of the results reveals that the bias is reduced in FDRS during winter especially north of the CAA and Greenland where a more complex topography exists with a maximum presence of ridges and keels as seen in Section 3.b. Overall, the vdiff errors are larger in FDRS than in CNDS. This is especially true in the Beaufort region where the ice drift is much faster leading to notable magnitude and directional differences between the simulated and observed velocities. We also observe significantly larger vdiff in FDRS north of the CAA especially during the summer season. At this stage, the cause (forcing, rheology, etc.) of the rapid shift in the bias at the end of the summer season is still unclear. This will be examined in the following sections.

Results from a comparison between ASITS data and the model are presented in Fig. 9 and show, in general, similar behaviour to that found from IABP buoy data. Indeed, we note an increase in the ice velocity bias between spring and summer followed by an abrupt decrease at the end of summer. In addition, the mean ice velocity bias from FDRS is slightly higher than that from CNDS (-1.39 cm s^{-1} and -1.70 cm s^{-1}, respectively) because of faster simulated drift in summer. This result confirms the finding from the IABP data comparison, revealing clearly that the form drag parameterization accelerates the ice in summer. As with IABP buoy data, vdiff is higher in summer for FDRS than for CNDS.

In the following subsections, the analysis focuses on results obtained when using IABP buoy data for validation because

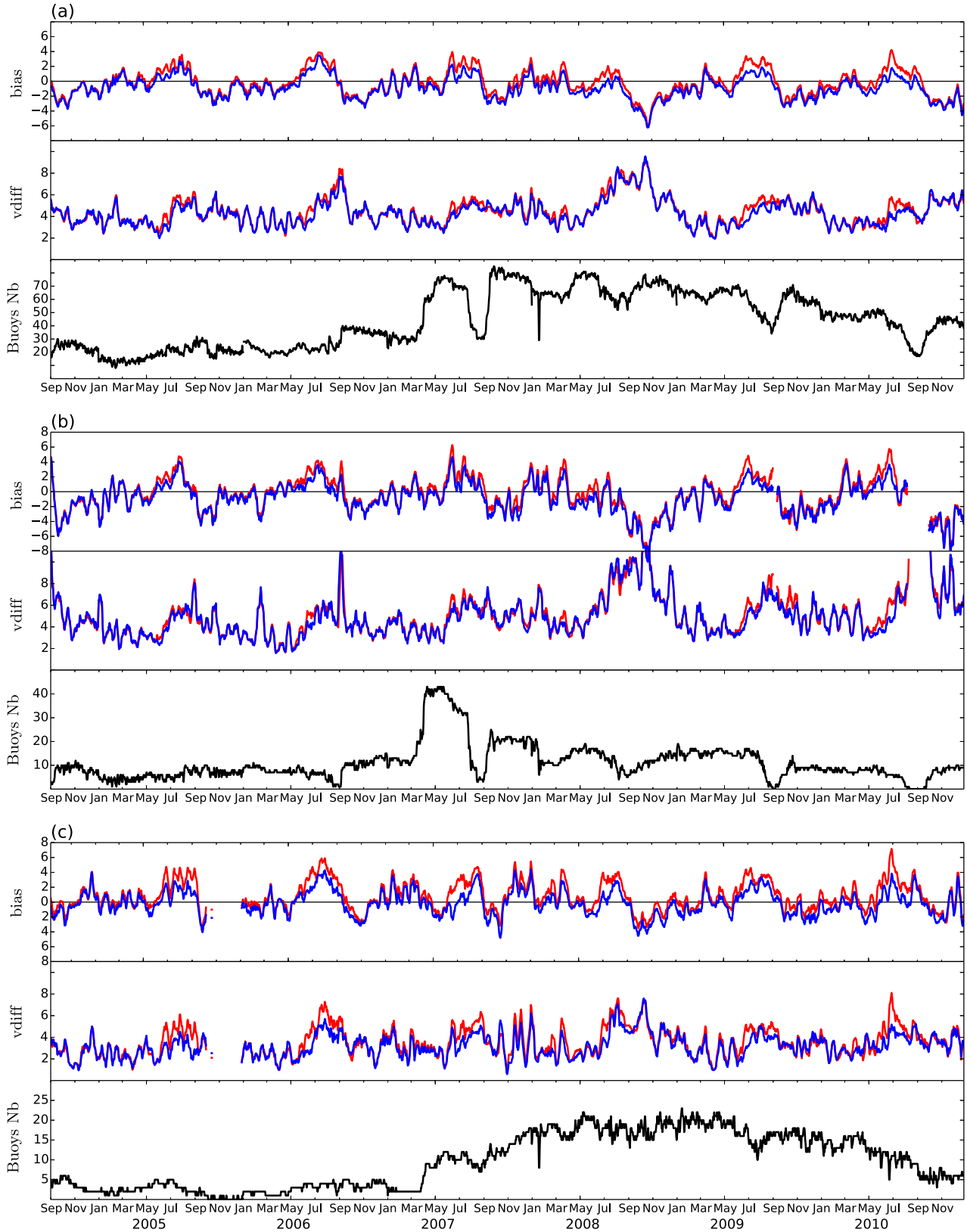

Fig. 8 10-day moving average (cm s^{-1}) of ice velocity mean bias (bias) and ice velocity deviation (vdiff), computed for FDRS (red) and CNDS (blue) considering buoys over (a) the entire Arctic, (b) the Beaufort Sea region, and (c) north of the Canadian Arctic Archipelago and Greenland. Buoy numbers are also shown in black.

TABLE 1. Statistics of FDRS simulation ice velocity (cm s^{-1}) validated using IABP buoy data.

	bias		vdiff	
FDRS Simulation	Winter	Summer	Winter	Summer
Arctic	−0.97	1.76	4.36	5.34
North of CAA and Greenland	0.12	2.75	3.26	4.81
Beaufort Sea region	−0.93	2.08	4.62	6.02

TABLE 2. As in Table 1 but for CNDS.

	bias		vdiff	
CNDS Simulation	Winter	Summer	Winter	Summer
Arctic	−1.50	0.52	4.32	4.82
North of CAA and Greenland	−0.75	1.10	3.11	3.90
Beaufort Sea region	−1.38	1.06	4.57	5.65

they are deemed to be of good quality and cover larger parts of the Arctic, such as north of the CAA and Greenland, compared with ASITS data.

Additionally, the bias diagnostic can be looked at from a spatial perspective. This is presented in Fig. 10 in which the spatial distribution of the velocity bias is shown through the geographical positions of the buoys considered in our diagnostic for the months of January (Figs 10a and 10c) and July (Figs 10b and 10d). Figure 10a represents results from FDRS for January and shows that the model exibits a slightly negative bias over most of the domain with some exceptions north of the CAA. Figure 10c shows the corresponding bias for the CNDS and reveals similar patterns with, however, lower biases, especially north of the CAA. In July, an overall positive bias is observed in FDRS, especially north of Greenland, north of the CAA, and along the Alaskan coast indicating that the drift in this Beaufort Gyre branch is too strong (Fig. 10b). This positive bias is less evident in the CNDS counterpart (Fig. 10d) with the ice drift being significantly slower in both regions.

These first results shown in Figs 8 and 10 reveal some issues in the ice velocity predicted by the model with a systematic positive bias being observed during the summer period followed by a shift to a negative bias in fall when the ice begins to form and strengthen. During the summer period, the ice drift is mostly driven by the ice–atmosphere and ice–ocean stresses. These two stresses are increased in FDRS in comparison to those from CNDS (not shown) with the highest differences observed north Greenland and the CAA. Because both FDRS and CNDS exhibit a positive bias in summer, we first explore whether the CGRF wind forcing is too strong during this season.

To explore this potential issue, a comparison is made between winds from the CGRF's forcing data and those from the European Centre for Medium-range Weather Forecasts (ECMWF) interim reanalysis (ERA-Interim) (Dee et al., 2011). The wind data come from consecutive 6 h forecasts (from CGRF and

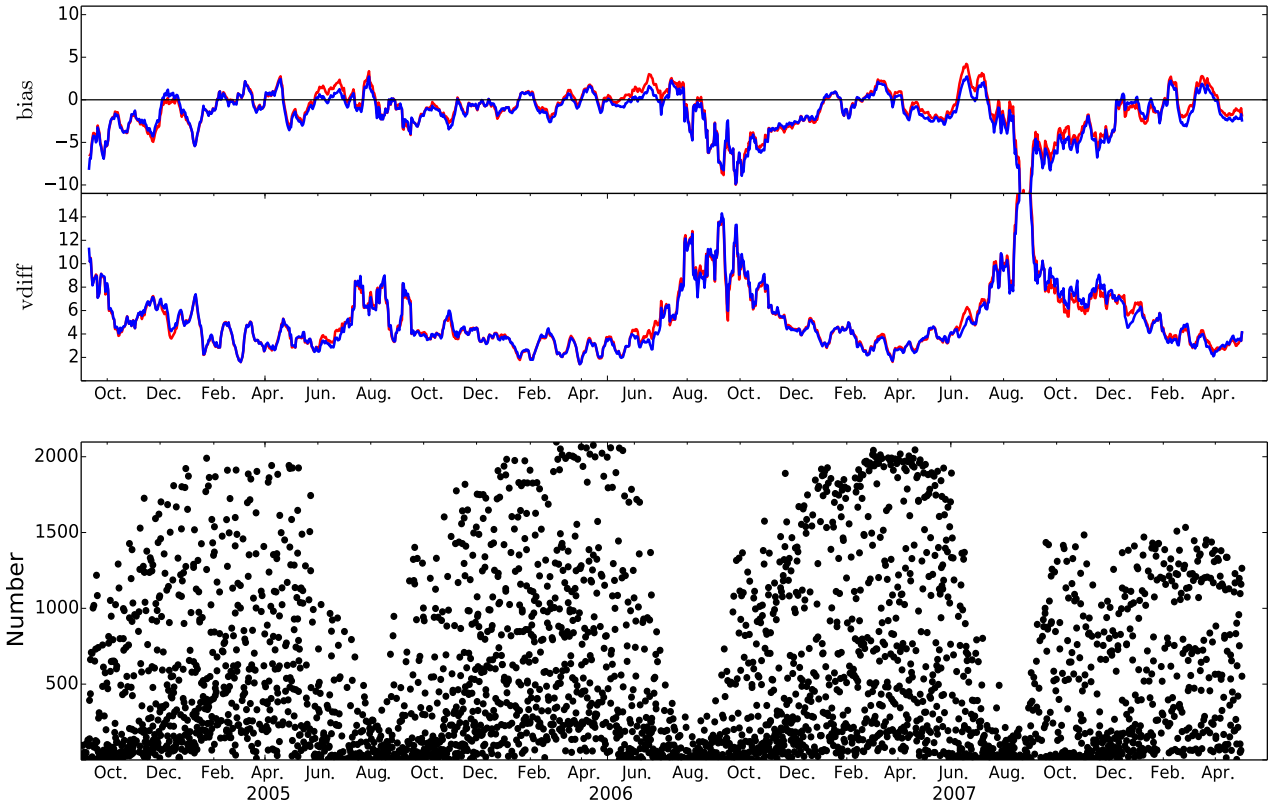

Fig. 9 As in Fig. 8 but using Automated Sea Ice Tracking System (ASITS) data. The bottom plot denotes the number of all displacements considered. See text for details on ASITS data coverage.

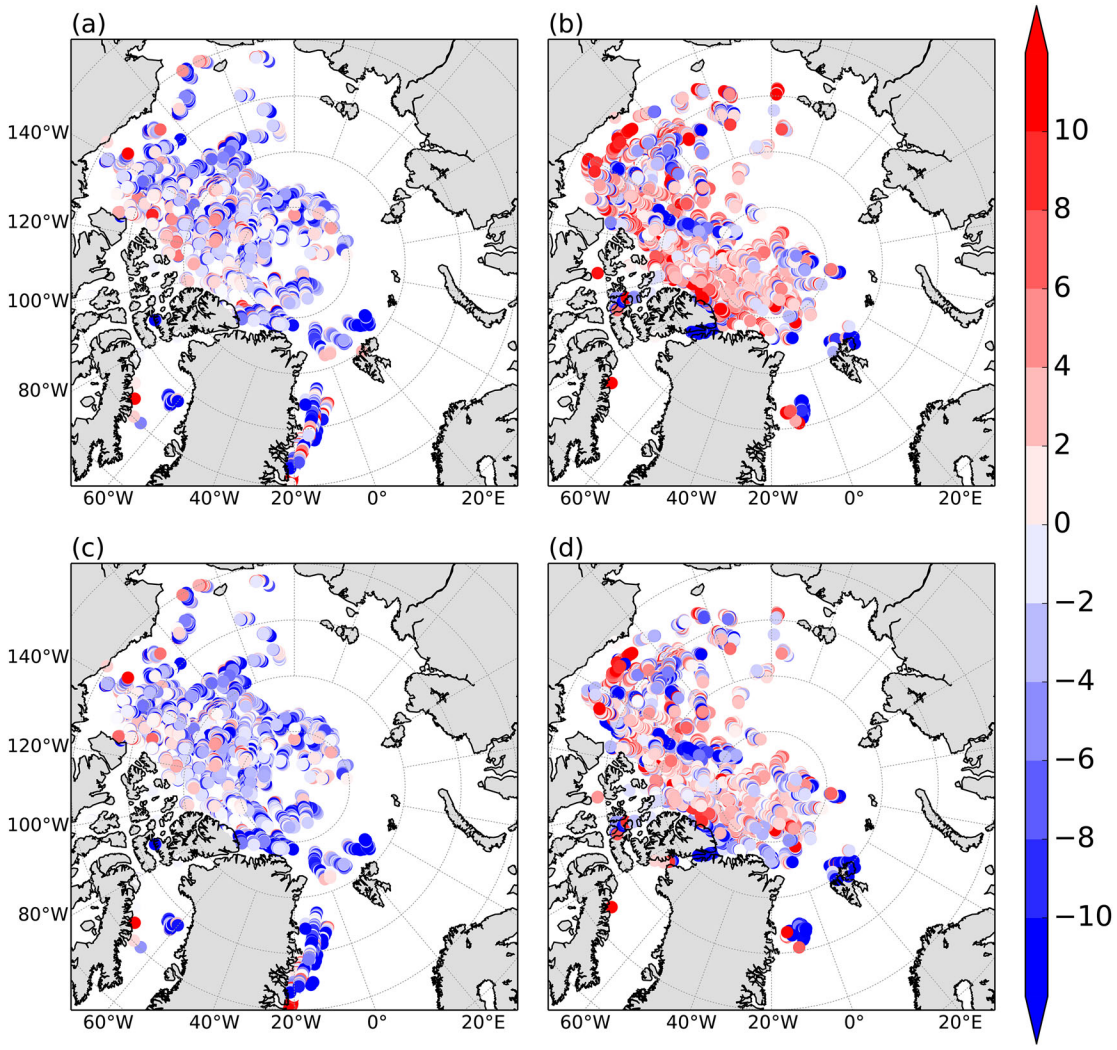

Fig. 10 Velocity bias (cm s^{-1}) at all buoy positions considered for (a) and (c) January and (b) and (d) July. The upper panels represent FDRS while the lower panels represent CNDS.

ERA-Interim reanalyses) throughout a one-year period. We chose the year 2010 and consider this period long enough to ensure a significant comparison. Figure 11 shows that the wind speeds from the two datasets are similar and do not exhibit significant differences (generally less than 0.5 m s^{-1} with a mean difference of 0.06 m s^{-1}). Although not a direct evaluation of wind errors, the comparison with ERA-Interim does suggest that there are no obvious biases in CGRF

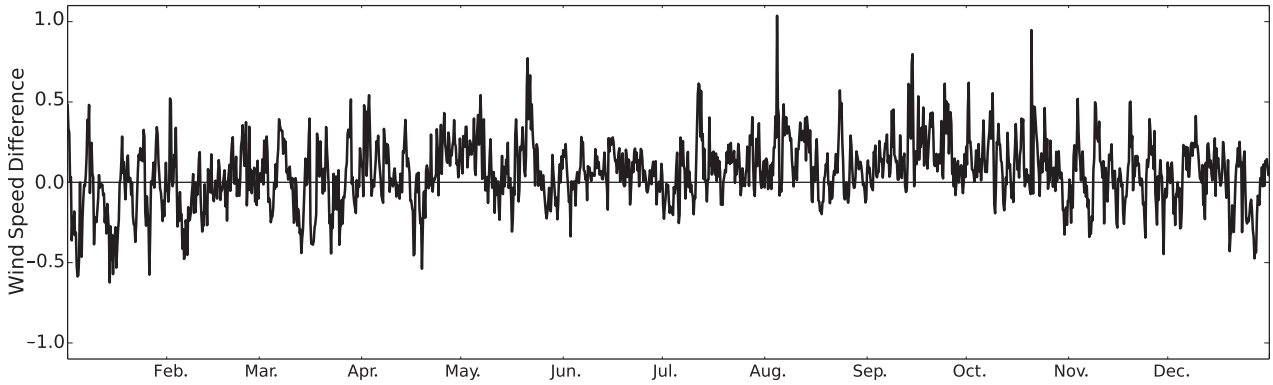

Fig. 11 Difference between GEM forcing winds speed and ERA-Interim reanalyses wind speed (m s^{-1}) at 10 m height ($|\mathbf{V}_{GEM}| - |\mathbf{V}_{ERA}|$) computed every consecutive 6 h throughout the year 2010. The spatial averaging is performed over the Arctic region north of 60°N.

forcing. In other words, it appears unlikely that CGRF wind forcing causes the observed summer positive bias in the model.

Other hypothetical factors can cause the summertime positive bias, such as an overly high ice–atmosphere drag coefficient leading to excessive ice–atmosphere stress. Similarly, it could also result from an overly low ice–ocean drag coefficient inducing a weak ice–ocean stress that does not produce a sufficient braking effect on the ice. A deeper examination of these hypotheses is presented in the next subsection. From now on, only the reference simulation (FDRS) is analyzed.

d *Sensitivity to Form Drag Scheme Modifications*

The cause of the summertime positive bias is examined by performing sensitivity tests in which the form drag parameterization is modified. Our results show that the neutral drag contribution from the melt ponds can be important in summer and even exceed 20% of the total drag in some regions. An example is illustrated in Fig. 12 showing the different drag contributions interpolated to buoy positions located north of the CAA and Greenland. In the first sensitivity experiment, we explore the significance of the contribution of the melt ponds to the total form drag. This is achieved by performing a simulation in which the ice–atmosphere drag is computed while ignoring the contribution from the edge of the melt pond. In another sensitivity experiment, the ratio of the mean ridge height and the mean keel depth ($R_h = H_k/H_r$) used in the parameterization scheme is modified from its default value ($R_h = 4$) to $R_h = 6$. This is to increase the keel drag with respect to ridges and favour a more effective ice–ocean stress.

Results obtained from these sensitivity tests are presented in Fig. 13. As expected, ignoring the effect of melt ponds in the total neutral drag coefficient is only perceptible in summer. This can be seen in Fig. 13 in which the black and blue lines are virtually indistinguishable outside the summer period. It is shown, however, that ignoring melt ponds reduces the positive summertime bias with a more notable impact north of the CAA and Greenland. This indicates that the ice morphology, as well as the ice characteristics, in this subregion favour the formation of ice melt ponds. This is also suggested in Fig. 6b. Results also show no significant impact on vdiff. Modification of the R_h ratio from 4 to 6 notably increases the ice–ocean stress braking effect resulting in lower ice velocities. However, even when the summertime positive bias was reduced, the modified R_h ratio introduced a

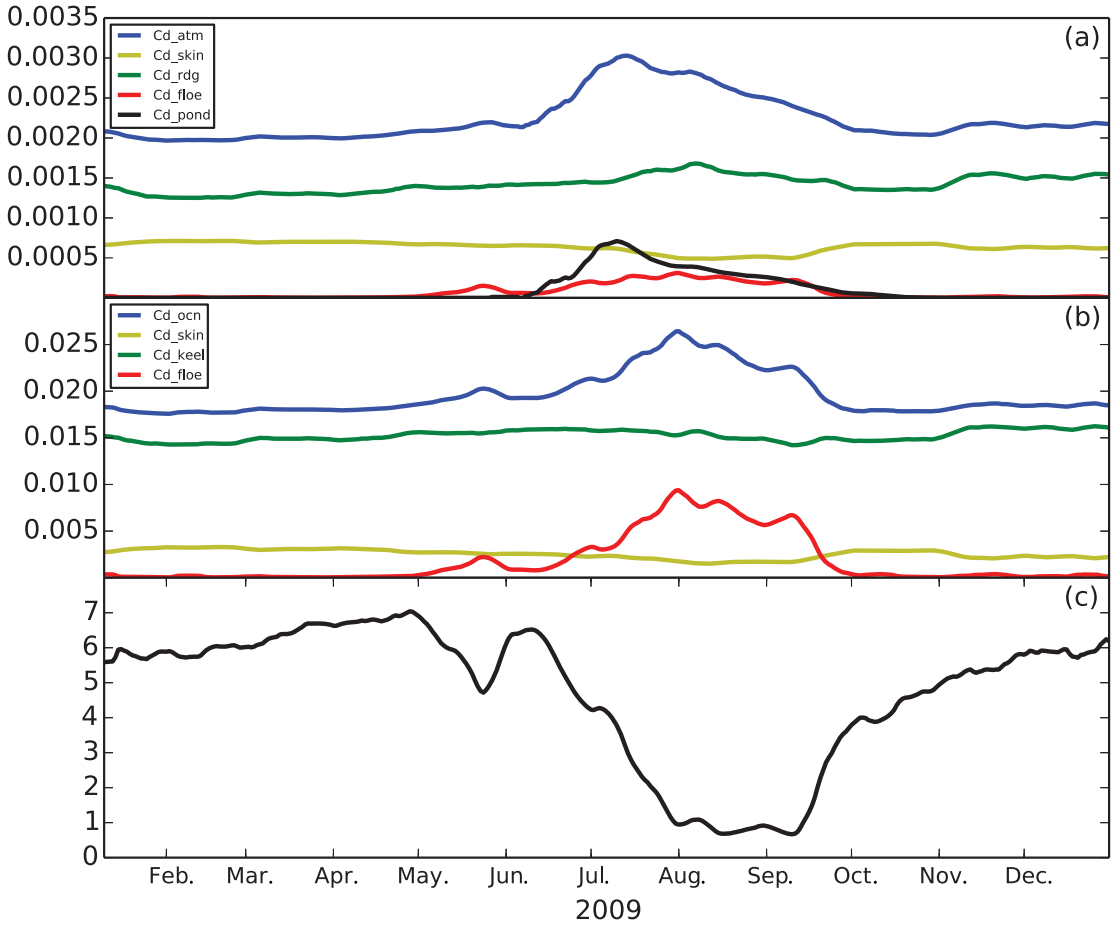

Fig. 12 10-day mean averages of mean neutral drag coefficients and ice strength interpolated to buoy positions in the region north of the CAA and Greenland throughout 2009. (a) Ice–atmosphere interface neutral drag coefficients and (b) ice–ocean interface. (c) Ice strength in 10^4 N m^{-1}. Colour coding and legend definitions for panels (a) and (b) are identical to those in Fig. 5.

systematic lower ice velocity throughout the year and over all subregions resulting in a systematic shift in the bias. Even though the ratio modification leads to small improvements in vdiff, it does not alleviate the summer bias issue.

The velocity bias diagnostics as shown in Section 3.c show a positive bias in summer followed by a rapid shift to negative values in early fall in both FDRS and CNDS. This suggests that factors other than the formulation of the drag coefficients can explain this behaviour. In the following, we investigate the potential effect of the ice strength formulation on ice drift through its impact on the internal stress gradient. Indeed, we can argue that an overly weak internal stress gradient could lead to higher ice velocity. Additionally, it is found from Fig. 12 that a decrease in ice strength beginning in May is associated with the onset of the contribution from the floe edge to the total drag. In other words, an overly weak ice cover could more easily fail, revealing cracks and leads that could enhance the contribution from the floe edge to the total drag and, therefore, further increase the ice velocity in FDRS. In contrast, this contribution drops rapidly when the ice becomes stronger through the formation of new ice in September. It is, therefore, clear that the way in which ice strength is parameterized notably affects the simulated ice velocity.

In the next subsection, we introduce new sensitivity tests related explicitly to the ice strength formulation used in CICE.

e *Impact of the Strength Formulation on the Ice Velocity*

As mentioned previously, in our sea-ice model CICE ice strength is represented using the Hibler formulation (Hibler, 1979) as follows,

$$P = P^* h \exp[-C(1-A)], \tag{12}$$

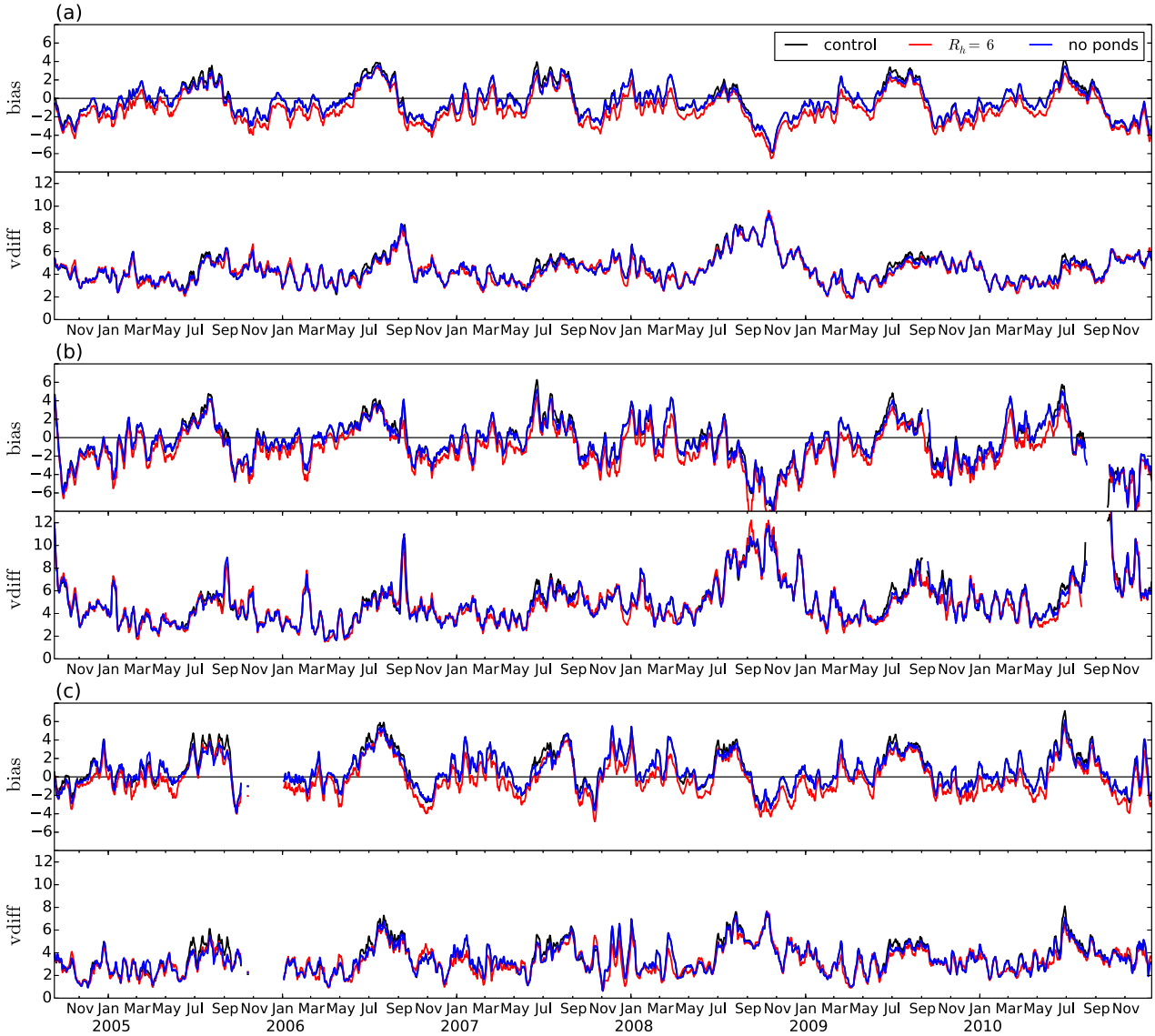

Fig. 13 As in Fig. 8 but resulting from sensitivity tests on the form drag scheme. The blue line represents the simulation in which the melt pond edge effect is ignored; the red line is the simulation in which $R_h = 6$, and the black line is the reference.

where h is mean ice thickness, A is ice concentration, and P^* and C are empirical constants. In the default model setup P^* and C are set to 2.75×10^4 N m^{-2} and 20, respectively.

In the following, we will explore how the simulated sea-ice drift can be improved by modifying the ice strength formulation. The ice strength as expressed in Eq. (12) can be modified through the two parameters P^* and C. Knowing that the ice velocity bias as shown in Fig. 8 presents generally positive values in summer and shifts to negative values in fall, an increase in P^* will strengthen the ice and slow its velocity leading to a reduced positive bias in summer. Unfortunately, this ice slowing will also exacerbate the negative bias in fall and winter. In contrast, the other parameter C is related to ice concentration and thus, will not alter the ice strength in the same manner throughout the year. For each model grid point, the impact of the C

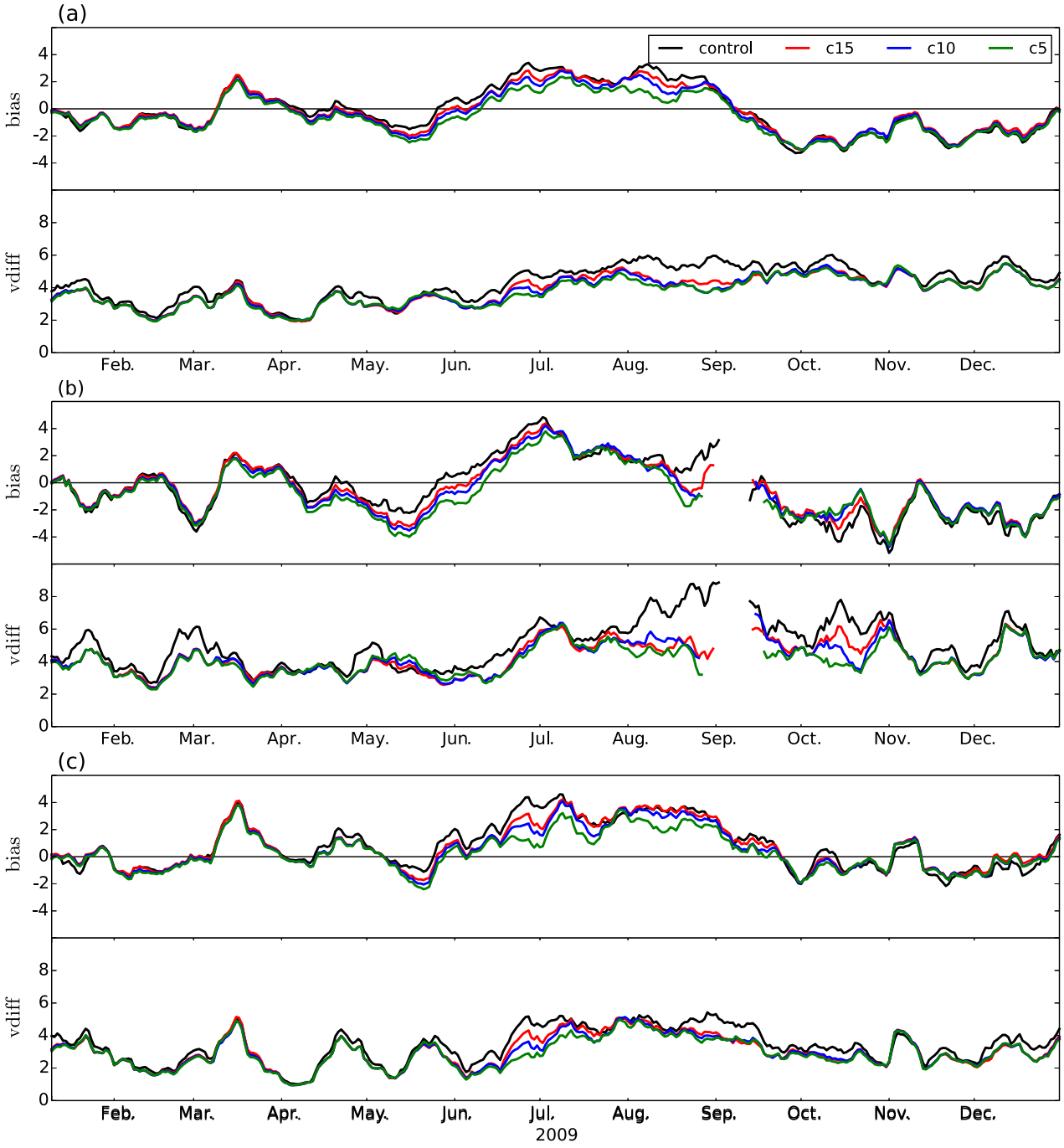

Fig. 14 10-day moving average (cm s^{-1}) of ice velocity mean bias (bias) and ice velocity deviation (vdiff) resulting from sensitivity tests for different C values in the ice strength Hibler formulation (Eq. (12)). $C = 20$ (black line control), $C = 15$ (red line), $C = 10$ (blue line), and $C = 5$ (green line). Buoys are considered over (a) the entire Arctic, (b) the Beaufort Sea region, and (c) north of the Canadian Arctic Archipelago and Greenland.

parameter on ice strength is much less important when the ice concentration is high and approaches 100%. Having higher ice concentration in fall and winter and lower cover in summer it, therefore, appears more suitable to modify ice strength through the C parameter rather than altering P^*. In addition, Ungermann et al. (2017) performed optimization tests on the Hibler ice strength formulation by tuning the parameters P^* and C. Through their minimization procedure, they found that $C = 15.92$ is an optimal value.

To examine the impact of ice strength on ice dynamics and, hence, on its velocity, several tests were conducted using different values of the C parameter in Eq. (12). Indeed, ice is gradually strengthened by setting $C = 15$, $C = 10$, and $C = 5$. Note also that these new sensitivity simulations started from the end of 2008 and cover a one-year period (2009). These simulations all start from the same initial conditions (a restart file from the standard FDRS simulation described in Section 2). Results are presented in Fig. 14 and show significant changes in the velocity bias as well as in vdiff. In general, decreasing C lowers the modelled ice velocity and reduces the summer bias and vdiff. The highest impact in summer is found north of Greenland and the CAA because of the thicker and more compact ice in these regions. In the Beaufort Sea region, the impact on bias is less apparent because of the rapid decrease in ice concentration (Fig. 15) as well as thinner ice cover in this region (not shown). We also note that varying the constant C in the ice strength formulation has an overall effect during the melting period from May to July. Indeed, during these months, ice concentration drops gradually but remains high (more than 85%) leading to the most effective ice strength increase resulting from a change in C.

In Hibler's formulation (Eq. 12), the ice strength P depends only on mean thickness h and concentration A. Lipscomb, Hunke, Maslowski, and Jakacki (2007) mentioned that the ice strength is weaker in pack ice of heterogeneous thicknesses (with thin and thick ice) compared with pack ice with homogeneous thicknesses. This suggests that Hibler's parameterization may, in some cases, lead to excessive ice strength. Instead, Hibler (1980) and Hopkins (1998) propose that the ice strength P should be proportional to $h^{3/2}$. Following these remarks, we tested a new variant of the ice strength parameterization based on Eq. (13). The idea is to respectively weaken and strengthen the ice pack below and above a certain thickness threshold. The aim is to accelerate the newly formed thinner ice in fall and decelerate the multi-year thicker ice. In this way, the ice velocity bias can be improved in summer as well as in fall.

The new formulation is as follows:

$$P = P^*_{\text{new}}\, h^{3/2}\, \exp\left[-C(1-A)\right], \tag{13}$$

where P^*_{new} can be obtained by assuming that the two formulations (Eqs (12) and (13)) are equivalent for a certain mean ice thickness. From our simulations, we obtain a mean ice thickness of roughly 2 m over the Beaufort Sea and north of the CAA and Greenland. Consequently, the following expression is deduced,

$$P = \frac{P*}{\sqrt{2}}\, h^{3/2}\, \exp[-C(1-A)]. \tag{14}$$

Results from different ice strength formulations are presented in Fig. 16 where the new expression (Eq. (14)) is used with different values of the C parameter. Figure 16 shows that the modified Hibler formulation significantly reduces ice velocity for the period from the beginning of ice melting until the end of summer (April–August), which improves the summer season positive bias. An important remark is that the modified Hibler formulation tends to accelerate ice drift in autumn and winter especially in the Beaufort Sea region. The negative bias observed in the reference version is, therefore, reduced (i.e., less negative). These results could be explained by the fact that, for relatively thin ice thickness (less than 2 m), such as newly formed ice, the

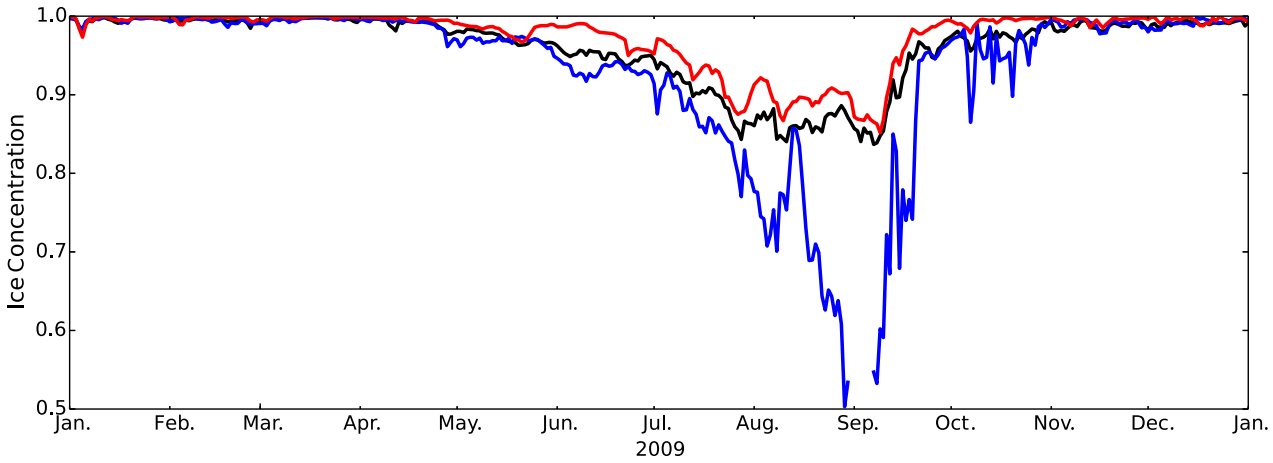

Fig. 15 Mean ice concentration at buoy positions when considered over the entire Arctic (black line), over the Beaufort Sea region (blue line), and north of the Canadian Arctic Archipelago and Greenland (red line). Ice concentrations are interpolated from the reference simulation.

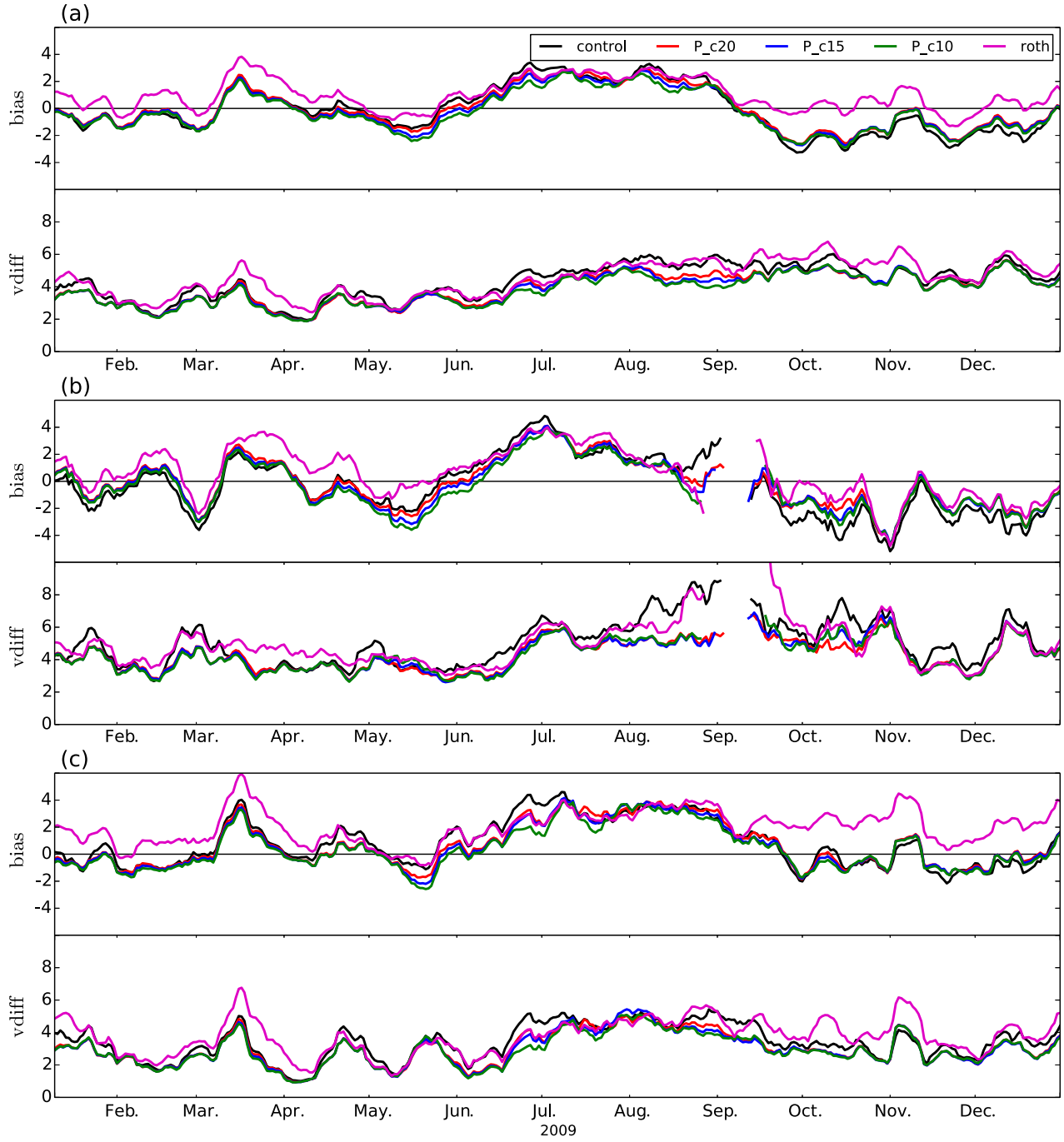

Fig. 16 As in Fig. 14 but resulting from sensitivity tests for different ice strength formulations. The standard Hibler formulation (Eq. (12)) is in black; the modified Hibler formulation (Eq. (14)) is in brown, blue, and green for which C parameter values are 20, 15, and 10, respectively. The additional experiment in which the Rothrock formulation is used is shown in magenta. Buoys are considered over (a) the entire Arctic, (b) the Beaufort Sea region, and (c) north of the Canadian Arctic Archipelago and Greenland.

modifed formulation makes the ice strength weaker and favours a faster ice velocity. On the contrary, when the pack ice is thicker (more than 2 m), such as the multi-year ice predominant to the north of the CAA and Greenland, the new strength formulation makes it stronger, and the drift is decelerated. In the case of the Rothrock formulation (Rothrock, 1975) (magenta line in Fig. 16), the ice velocity is substantially increased throughout the year except for the summer period. Moreover, the relatively low bias observed over the Arctic from September to the end of the year is misleading in the sense that it results from compensating negative and positive biases, respectively, in the Beaufort Sea and north of the CAA and Greenland. It is noted here that the bias optimization previously achieved was applied to the model using the

Hibler formulation. Therefore, results from simulations using the Rothrock formulation cannot be fairly compared with those for which the Hibler ice strength was used.

4 Conclusions

In this study, a regional coupled prediction system based on CICE–NEMO was examined through its performance in simulating ice velocity. The data used to validate the simulated ice velocity came from buoy positions provided by the IABP, as well as ASITS. The first part of the study was dedicated to investigating the impact of including a form drag parameterization (Tsamados et al., 2014). In this parameterization, neutral drag coefficients for ice–atmosphere and ice–ocean interfaces were defined through contributions from different ice topographic features. Namely, ridges, keels, freeboard, draft, melt ponds, and finally level ice. These neutral drag coefficients are retrieved from model prognostic variables, such as ice concentration, thickness, and ridged volume. A reference hindcast simulation (FDRS) revealed that, on average, the predominant contribution to the total neutral drag coefficient came from ridges and keels, with a maximum occuring in June. The spatial distribution indicated that maximum values are found not only north of the CAA and Greenland but also offshore of the Alaskan coast.

Ice velocity diagnostics, such as bias and velocity deviation vdiff (defined in Section 2.b), were used to assess the introduction of the form drag parameterization to the model. This was done by comparing simulated ice velocity diagnostics with those resulting from a simulation in which the neutral drag coefficients were kept constant (CNDS). First results revealed that the form drag parameterization systematically increased ice velocity compared with CNDS. This is consistent with the results of Castellani et al. (2018). This is most noticeable in summer in the region to the north of the CAA and Greenland. Unlike the improvement observed in summer sea-ice drift found by Castellani et al. (2018) and Steiner (2001), this acceleration in ice velocity exacerbates a positive bias already present in the simulation in which the neutral drag coefficients are fixed.

In an attempt to understand the cause(s) of the positive bias in the summer period, the atmospheric wind forcing was compared with ERA-Interim reanalyses for a one-year period and were found to be similar. This led us to discard the hypothesis that overly strong winds produced excessive ice–atmosphere stresses. On the other hand, another sensitivity simulation was performed in which the melt pond drag effect was tested by ignoring its contribution to the total neutral drag coefficient. Although slightly reduced, the summertime positive bias was still present, and the melt pond drag effect did not seem to be the cause of this overly fast ice velocity. The compensating effect between ice–atmosphere stress and ice-ocean stress was also evaluated by increasing the ratio between the mean keel depth and mean ridge height from 4 to 6. Results from this test revealed a systematic decrease in ice velocity throughout the year, not only in summer.

The second part of this work was devoted to studying the effect of ice strength on ice velocity. First, the ice strength was increased by modifying the C empirical parameter in the Hibler formulation used by default in the model. Results from these sensitivity tests, applied over a one-year period, showed a relative decrease in ice velocity with increasing ice strength with the effect being stronger in summer, mostly north of the CAA and Greenland probably because of the thicker ice in these regions. The experimentation was extended further to test the ice strength formulation itself. Indeed, the linear relation between ice strength and mean ice thickness changed to a function proportional to $h^{3/2}$ as defined in Eq. (13). This modified formulation reduced the positive summertime bias. It also reduced the negative bias observed in fall and winter, with a more noticeable effect in the Beaufort Sea region.

There are some indicators, such as a somewhat lower total ice volume relative to other reference simulations, such as that of Tsamados et al. (2014), that point toward a slight overestimation of melting in our simulation. This could contribute, in particular, to lower ice concentrations during summer leading to a weaker ice cover and higher velocities as consequences. Hence, it should be recognized that the results presented above could be modulated by the simple play of thermodynamics. We acknowledge this factor but raise the difficulty of obtaining accurate measurements of summertime ice concentration. Significant summer differences between remotely sensed products, such as those from NSIDC (Fowler et al. 2013) and the Hadley Centre Sea Surface Temperature dataset (HadSST; Rayner et al. (2006)) to take the most often used ones, usually a question of the fraction of ponded sea ice being interpreted as open water, illustrates this general level of uncertainty. Therefore, even if our model is likely to be slightly on the warm side of the range, we believe that the sensitivity experiments carried out in the present study show some interesting avenues for improving ice drift in general. Some parameters, such as C in the Hibler ice strength formulation, were defined for convenience and do not carry any precise physics except a crude empirical idea that the ice strength must decrease quickly as the concentration is reduced. The same could be said about the linear relationship in Hibler's formulation between mean thickness and strength.

Another source of uncertainty in the ice–ocean coupling is the robustness of the representation of the ocean surface turbulence and the mixed layer in summer (melt period; i.e., shallow mixed layer and strongly stratified ocean) and winter (convection period under the ice due to brine rejection and an associated deeper mixed layer) because the depth of the mixed layer directly affects the extent of the braking the ocean can have over the ice. Both periods are still, in fact, crudely represented in ocean models, which tend to be overly mixed in summer and for which the representation of the brine rejection is still a matter of research. For instance, a less turbulent and thinner summer melt layer would even exacerbate the summer velocity bias that we have found, a process absent in CICE stand-alone runs performed by Tsamados et al. (2014). All in all, ice–ocean

coupling happens to be more treacherous than expected, some feedback via the stratification and turbulence of the ocean possibly complicating the general idea that the form drag parameterization causes an increase in atmosphere–ice summer drag that, in turn, causes an increase in velocity (the associated increase in ice–ocean drag playing a lesser role).

In summary, the new form drag parameterization, although more physically realistic, is found to exacerbate a positive ice velocity bias in summer already present in the previous version of the CICE model in which the neutral drag coefficient is kept constant. This result indicates that the new form drag scheme, which makes several assumptions and includes many free parameters, requires more investigation in order to obtain robust and reliable improvements. Modifications in the ice strength formulation and the parameters used also produce significant changes in ice drift simulation. This indicates that significant uncertainties remain in the ice strength parameterization, and additional work is needed to examine this issue more deeply. It is noted that other aspects of the model need to be examined when implementing variable atmosphere–ice and ice–ocean drag coefficients. Indeed, the impact on ice thickness can be assessed in terms of potential biases. Also, the impact of a higher horizontal resolution, such as that used in RIOPS, can be examined in the context of a variable drag coefficient. Another interesting aspect to look at might be a higher resolution forcing wind that would better represent small scales. We point out that changing the drag coefficients for the ice–atmosphere interface without changing the winds creates inconsistencies in momentum fluxes. Future work is needed to examine this issue in the context of a fully coupled atmosphere–ice–ocean system.

Acknowledgements

The IABP data are made available at http://iabp.apl.washington.edu/. The ASITS data can be made available by contacting Mike Brady (Mike.Brady@canada.ca). The ERA-Interim data are provided through the ECMWF data server https://www.ecmwf.int/en/forecasts/datasets/. The CICE–NEMO code and the Environment and Climate Change Canada atmospheric forcing data used for the numerical experiments are available upon request. The NSIDC sea-ice concentration data can be obtained at http://nsidc.org/data/seaice_index/. The ICESat sea-ice thickness data are available at https://nsidc.org/data/icesat. The NSIDC sea-ice drift can be obtained at https://nsidc.org/data/nsidc-0116/versions/2. The first author benefited from a visiting fellowship from the Natural Sciences and Engineering Research Council of Canada and funding from the Program of Energy Research and Development.

Disclosure statement

No potential conflict of interest was reported by the authors.

ORCID

Stephen E. L. Howell http://orcid.org/0000-0002-4848-9867

References

Bouchat, A., & Tremblay, B. (2014). Energy dissipation in viscous-plastic sea-ice models. *Journal of Geophysical Research: Oceans*, *119*(2), 976–994.

Bouchat, A., & Tremblay, B. (2017). Using sea-ice deformation fields to constrain the mechanical strength parameters of geophysical sea ice. *Journal of Geophysical Research: Oceans*, *122*(7), 5802–5825.

Castellani, G., Losch, M., Ungermann, M., & Gerdes, R. (2018). Sea-ice drag as a function of deformation and ice cover: Effects on simulated sea ice and ocean circulation in the Arctic. *Ocean Modelling*, *128*, 48–66.

Castellani, G., Lüpkes, C., Hendricks, S., & Gerdes, R. (2014). Variability of Arctic sea-ice topography and its impact on the atmospheric surface drag. *Journal of Geophysical Research: Oceans*, *119*(10), 6743–6762.

Charron, M., Polavarapu, S., Buehner, M., Vaillancourt, P., Charette, C., Roch, M., … Heillette, S. (2012). The stratospheric extension of the Canadian global deterministic medium-range weather forecasting system and its impact on tropospheric forecasts. *Monthly Weather Review*, *140*(6), 1924–1944.

Côté, J., Desmarais, J.-G., Gravel, S., Méthot, A., Patoine, A., Roch, M., & Staniforth, A. (1998b). The operational CMC–MRB global environmental multiscale (GEM) model. Part II: Results. *Monthly Weather Review*, *126* (6), 1397–1418.

Côté, J., Gravel, S., Méthot, A., Patoine, A., Roch, M., & Staniforth, A. (1998a). The operational CMC–MRB global environmental multiscale (GEM) model. Part I: Design considerations and formulation. *Monthly Weather Review*, *126*(6), 1373–1395.

Dee, D. P., Uppala, S., Simmons, A., Berrisford, P., Poli, P., Kobayashi, S., … Vitart, F. (2011). The ERA-Interim reanalysis: Configuration and performance of the data assimilation system. *Quarterly Journal of the Royal Meteorological Society*, *137*(656), 553–597.

Dupont, F., Chittibabu, P., Fortin, V., Rao, Y. R., & Lu, Y. (2012). Assessment of a NEMO-based hydrodynamic modelling system for the Great Lakes. *Water Quality Research Journal*, *47*(3–4), 198–214.

Dupont, F., Higginson, S., Bourdallé-Badie, R., Lu, Y., Roy, F., Smith, G. C., … Davidson, F. (2015). A high-resolution ocean and sea-ice modelling system for the Arctic and North Atlantic oceans. *Geoscientific Model Development*, *8*(5), 1577–1594.

Durnford, D., Fortin, V., Smith, G. C., Archambault, B., Deacu, D., Dupont, F., … Dickout, J. (2018). Towards an operational water cycle prediction system for the Great Lakes and St. Lawrence River. *Bulletin of the American Meteorological Society*, *99*(3), 521–546.

Ferry, N., Parent, L., Garric, G., Bricaud, C., Testut, C. E., Le Galloudec, O., … Molines, J. M. (2012, January). GLORYS2V1 global ocean reanalysis of the altimetric era (1992–2009) at meso-scale. *Mercator Quarterly Newsletter*, *44*, 28–39.

Flesch, T., D'Amours, R., Mooney, C., & Wilson, J. (2004). *MLDP*: *A long-range Lagrangian stochastic dispersion model* (Internal report of the Department of Earth and Atmospheric Sciences, University of Alberta and the Canadian Meteorological Centre, Environment Canada).

Fowler, C., Maslanik, J., Emery, W., & Tschudi, M. (2013). *Polar Pathfinder daily 25 km EASE-grid sea ice motion vectors, version 2*. Boulder, CO: National Snow and Ice Data Center.

Girard, L., Bouillon, S., Weiss, J., Amitrano, D., Fichefet, T., & Legat, V. (2011). A new modeling framework for sea-ice mechanics based on elasto-brittle rheology. *Annals of Glaciology*, *52*(57), 123–132.

Hakkinen, S., Proshutinsky, A., & Ashik, I. (2008). Sea ice drift in the Arctic since the 1950s. *Geophysical Research Letters*, *35*(19), L19704. doi:10.1029/2008GL034791

Hebert, D. A., Allard, R. A., Metzger, E. J., Posey, P. G., Preller, R. H., Wallcraft, A. J., … Smedstad, O. M. (2015). Short-term sea ice forecasting: An assessment of ice concentration and ice drift forecasts using the US Navy's Arctic Cap Nowcast/Forecast System. *Journal of Geophysical Research: Oceans*, *120*(12), 8327–8345.

Hibler, W. (1979). A dynamic thermodynamic sea ice model. *Journal of Physical Oceanography*, *9*(4), 815–846.

Hibler, W. (1980). Modeling a variable thickness sea ice cover. *Monthly Weather Review*, *108*(12), 1943–1973.

Hopkins, M. A. (1998). Four stages of pressure ridging. *Journal of Geophysical Research: Oceans*, *103*(C10), 21883–21891.

Howell, S. E., Wohlleben, T., Dabboor, M., Derksen, C., Komarov, A., & Pizzolato, L. (2013). Recent changes in the exchange of sea ice between the Arctic Ocean and the Canadian Arctic Archipelago. *Journal of Geophysical Research: Oceans*, *118*(7), 3595–3607.

Hunke, E. C., Lipscomb, W. H., Turner, A. K., Jeffery, N., & Elliott, S. (2015). CICE: The Los Alamos sea ice model documentation and software user's manual (technical report, LA-CC-06-012 Version 5.1). Los Alamos, NM: Los Alamos Natl. Lab.

Hutter, N., Losch, M., & Menemenlis, D. (2018). Scaling properties of Arctic sea ice deformation in a high-resolution viscous-plastic sea ice model and in satellite observations. *Journal of Geophysical Research: Oceans*, *123*(1), 672–687.

Komarov, A. S., & Barber, D. G. (2014). Sea ice motion tracking from sequential dual-polarization RADARSAT-2 images. *IEEE Transactions on Geoscience and Remote Sensing*, *52*(1), 121–136.

Kreyscher, M., Harder, M., Lemke, P., & Flato, G. M. (2000). Results of the sea ice model intercomparison project: Evaluation of sea ice rheology schemes for use in climate simulations. *Journal of Geophysical Research: Oceans*, *105*(C5), 11299–11320.

Kwok, R., Cunningham, G. F., Wensnahan, M., Rigor, I., Zwally, H. J., & Yi, D. (2009). Thinning and volume loss of the Arctic Ocean sea ice cover: 2003–2008. *Journal of Geophysical Research: Oceans*, *114*(C7), C07005. doi:10.1029/2009JC005312

Kwok, R., Spreen, G., & Pang, S. (2013). Arctic sea ice circulation and drift speed: Decadal trends and ocean currents. *Journal of Geophysical Research: Oceans*, *118*(5), 2408–2425.

Kwok, R., & Untersteiner, N. (2011). The thinning of Arctic sea ice. *Physics Today*, *64*(4), 36–41.

Lemieux, J.-F., Dupont, F., Blain, P., Roy, F., Smith, G. C., & Flato, G. M. (2016). Improving the simulation of landfast ice by combining tensile strength and a parameterization for grounded ridges. *Journal of Geophysical Research: Oceans*, *121*(10), 7354–7368.

Lemieux, J.-F., Lei, J., Dupont, F., Roy, F., Losch, M., Lique, L., & Laliberté, F. (2018). The impact of tides on simulated landfast ice in a pan-Arctic ice-ocean model. *Journal of Geophysical Research: Oceans*, *123*, 7747–7762.

Lipscomb, W. H., Hunke, E. C., Maslowski, W., & Jakacki, J. (2007). Ridging, strength, and stability in high-resolution sea ice models. *Journal of Geophysical Research: Oceans*, *112*(C3), C03591. doi:10.1029/2005JC003355

Lüpkes, C., Gryanik, V. M., Hartmann, J., & Andreas, E. L. (2012). A parametrization, based on sea ice morphology, of the neutral atmospheric drag coefficients for weather prediction and climate models. *Journal of Geophysical Research: Atmospheres*, *117*(D13), D13112. doi:10.1029/2012JO017630

Madec, G. (2008). *NEMO reference manual, ocean dynamic component: NEMO-OPA* (no. 27). Note du Pôle de modélisation, France: Institut Pierre Simon Laplace.

Madec, G., Delecluse, P., Imbard, M., & Lévy, C. (1998). *OPA 8.1 general circulation model reference manual* (no. 11, pp. 11–91), Note du Pôle de modélisation, France: Institut Pierre Simon Laplace.

Martin, T., Tsamados, M., Schroeder, D., & Feltham, D. L. (2016). The impact of variable sea ice roughness on changes in Arctic Ocean surface stress: A model study. *Journal of Geophysical Research: Oceans*, *121*(3), 1931–1952.

McPhee, M. G. (2002). Turbulent stress at the ice/ocean interface and bottom surface hydraulic roughness during the SHEBA drift. *Journal of Geophysical Research*, *107*(C10), 8037. doi:10.1029/2000JC000633

Petty, A. A., Tsamados, M. C., Kurtz, N. T., Farrell, S. L., Harbeck, J. P., Feltham, D. L., & Richter-Menge, J. A. (2016). Characterizing Arctic sea ice topography using high-resolution IceBridge data. *The Cryosphere*, *10*(3), 1161–1179.

Rayner, N., Brohan, P., Parker, D., Folland, D., Kennedy, J., Vanicek, M., … Tett, S. (2006). Improved analyses of changes and uncertainties in sea surface temperature measured in situ since the mid-nineteenth century: The HadSST2 dataset. *Journal of Climate*, *19*(3), 446–469.

Richter-Menge, J. A., & Farrell, S. L. (2013). Arctic sea ice conditions in spring 2009–2013 prior to melt. *Geophysical Research Letters*, *40*(22), 5888–5893.

Rigor, I., & Ortmeyer, M. (2004). The International Arctic Buoy Programme–monitoring the Arctic Ocean for forecasting and research. *Arctic Research of the United States*, *18*, 21.

Rothrock, D. (1975). The energetics of the plastic deformation of pack ice by ridging. *Journal of Geophysical Research*, *80*(33), 4514–4519.

Roy, F., Chevallier, M., Smith, G. C., Dupont, F., Garric, G., Lemieux, J.-F., … Davidson, F. (2015). Arctic sea ice and freshwater sensitivity to the treatment of the atmosphere-ice-ocean surface layer. *Journal of Geophysical Research: Oceans*, *120*(6), 4392–4417.

Schreyer, H., Sulsky, D., Munday, L., Coon, M., & Kwok, R. (2006). Elastic-decohesive constitutive model for sea ice. *Journal of Geophysical Research: Oceans*, *111*, C11526. doi:10.1029/200SJC003334

Schweiger, A., Lindsay, R., Zhang, J., Steele, M., Stern, H., & Kwok, R. (2011). Uncertainty in modeled Arctic sea ice volume. *Journal of Geophysical Research: Oceans*, *116*(C8), C00D06. doi:10.1026/2011JC007084

Smith, G. C., Bélanger, J.-M., Roy, F., Pellerin, P., Ritchie, H., Onu, K., … Deacu, D. (2018). Impact of coupling with an ice-ocean model on global medium-range NWP forecast skill. *Monthly Weather Review*, *146*(4), 1157–1180.

Smith, G. C., Roy, F., & Brasnett, B. (2013). Evaluation of an operational ice–ocean analysis and forecasting system for the Gulf of St Lawrence. *Quarterly Journal of the Royal Meteorological Society*, *139*(671), 419–433.

Smith, G. C., Roy, F., Mann, P., Dupont, F., Brasnett, B., Lemieux, J.-F., … Bélair, S. (2014). A new atmospheric dataset for forcing ice–ocean models: Evaluation of reforecasts using the Canadian global deterministic prediction system. *Quarterly Journal of the Royal Meteorological Society*, *140*(680), 881–894.

Smith, G. C., Roy, F., Reszka, M., Surcel Colan, D., He, Z., Deacu, D., … Lajoie, M. (2016). Sea ice forecast verification in the Canadian global ice ocean prediction system. *Quarterly Journal of the Royal Meteorological Society*, *142*(695), 659–671.

Steele, M., Zhang, J., Rothrock, D., & Stern, H. (1997). The force balance of sea ice in a numerical model of the Arctic Ocean. *Journal of Geophysical Research: Oceans*, *102*(C9), 21061–21079.

Steiner, N. (2001). Introduction of variable drag coefficients into sea-ice models. *Annals of Glaciology*, *33*, 181–186.

Stroeve, J. C., Serreze, M. C., Holland, M. M., Kay, J. E., Malanik, J., & Barrett, A. P. (2012). The Arctic's rapidly shrinking sea ice cover: A research synthesis. *Climatic Change*, *110*(3), 1005–1027.

Sumata, H., Lavergne, T., Girard-Ardhuin, F., Kimura, N., Tschudi, M. A., Kauker, F., … Gerdes, R. (2014). An intercomparison of Arctic ice drift products to deduce uncertainty estimates. *Journal of Geophysical Research: Oceans*, *119*(8), 4887–4921.

Tsamados, M., Feltham, D. L., Schroeder, D., Flocco, D., Farrell, S. L., Kurtz, N., … Bacon, S. (2014). Impact of variable atmospheric and oceanic form drag on simulations of Arctic sea ice. *Journal of Physical Oceanography*, *44*(5), 1329–1353.

Tsamados, M., Feltham, D. L., & Wilchinsky, A. (2013). Impact of a new anisotropic rheology on simulations of Arctic sea ice. *Journal of Geophysical Research: Oceans*, *118*(1), 91–107.

Ungermann, M., Tremblay, L. B., Martin, T., & Losch, M. (2017). Impact of the ice strength formulation on the performance of a sea ice thickness distribution model in the Arctic. *Journal of Geophysical Research: Oceans*, *122*(3), 2090–2107.